LIMNOLOGY and OCEANOGRAPHY

ASLO

Limnol. Oceanogr. 68, 2023, 525–543

doi: 10.1002/lno.12290

Interactions of bioactive trace metals in shipboard Southern Ocean incubation experiments

Shannon M. Burns[1*] **Randelle M. Bundy**[2] **William Abbott**[1,3] **Zuzanna Abdala**[4,5] **Alexa R. Sterling**[6] **P. Dreux Chappell**[4] **Bethany D. Jenkins**[6,7] **Kristen N. Buck**[1,8*]

[1]College of Marine Science, University of South Florida, St. Petersburg, Florida, USA
[2]School of Oceanography, University of Washington, Seattle, Washington, USA
[3]National Oceanic and Atmospheric Administration Marine Operations Center – Pacific, Newport, Oregon, USA
[4]Department of Ocean and Earth Sciences, Old Dominion University, Norfolk, Virginia, USA
[5]Office of Habitat Conservation, National Marine Fisheries Service, NOAA, Silver Spring, Maryland, USA
[6]Department of Cell and Molecular Biology, University of Rhode Island, Kingston, Rhode Island, USA
[7]Graduate School of Oceanography, University of Rhode Island, Narragansett, Rhode Island, USA
[8]College of Earth, Ocean, and Atmospheric Sciences, Oregon State University, Corvallis, Oregon, USA

Abstract

In the Southern Ocean, it is well-known that iron (Fe) limits phytoplankton growth. Yet, other trace metals can also affect phytoplankton physiology. This study investigated feedbacks between phytoplankton growth and dissolved Fe, manganese (Mn), cobalt (Co), nickel (Ni), copper (Cu), zinc (Zn), and cadmium (Cd) concentrations in Southern Ocean shipboard incubations. Three experiments were conducted in September–October 2016 near the West Antarctic Peninsula: Incubations 1 and 3 offshore in the Antarctic Circumpolar Current, and Incubation 2 inshore in Bransfield Strait. Additions of Fe and/or vitamin B_{12} to inshore and offshore waters were employed and allowed assessment of metal (M) uptake relative to soluble reactive phosphorus (P) across a wide range of initial conditions. Offshore, treatments of >1 nmol L^{-1} added Fe were Fe-replete, whereas inshore waters were already Fe-replete. Results suggest Mn was a secondary limiting nutrient inshore and offshore. No Fe-vitamin B_{12} colimitation was observed. Overall, M:P uptake in the incubations was closely related to initial dissolved M:P for Fe, Mn, Co, Ni, and Cd, and for Cu inshore. Final concentrations of Fe and Zn were similar across light treatments of the experiments despite very different phytoplankton responses, and we observed evidence for Co/Cd/Zn substitution and for recycling of biogenic metals as inventories plateaued. In dark bottles, the absence of Mn oxidation may have allowed more efficient recycling of Fe and other trace metals. Our results provide insight into factors governing trace metal uptake, with implications for phytoplankton community composition locally and preformed micronutrient bioavailability in Southern Ocean water masses.

Trace metals play an essential role in marine primary productivity as micronutrients for phytoplankton (Sunda 1989; Bruland et al. 1991; Morel and Price 2003). Iron (Fe) in particular limits phytoplankton growth across much of the Southern Ocean (de Baar et al. 1990; Martin et al. 1990*a*; Moore et al. 2001; de Baar 2005; Boyd et al. 2007), a region that plays a crucial role in global biogeochemical cycles of nutrients and carbon (Sarmiento et al. 2004). Offshore waters in the Antarctic Circumpolar Current (ACC) are severely Fe-limited during austral spring and summer (Martin et al. 1990*a*; Browning et al. 2021). In contrast, the shelf waters of the West Antarctic Peninsula (WAP) are elevated in Fe (Martin et al. 1990*b*; de Jong et al. 2012; Hatta et al. 2013) and typically Fe-replete (Martin et al. 1990b; Hopkinson et al. 2007), although addition of more Fe to these waters at other times of year can lead to elevated phytoplankton biomass (Buck et al. 2010).

Phytoplankton growth can be colimited by two nutrients simultaneously, and/or be serially limited by primary and then secondary limiting nutrients as the stress of one nutrient

*Correspondence: kristen.buck@oregonstate.edu; sburns4@usf.edu

Additional Supporting Information may be found in the online version of this article.

Author Contribution Statement: K.N.B., P.D.C., and B.D.J. conceived the study. K.N.B., R.M.B., P.D.C., and B.D.J. conducted the experiments at sea. All authors contributed to the sampling and analyses. S.M.B. synthesized the results and created all tables and figures. S.M.B. and K.N.B. wrote the manuscript with input from all authors. All authors edited and approved the final manuscript.

is relieved and another becomes limiting (Saito et al. 2008). Cobalt (Co)-containing B vitamins are produced by bacteria and archaea but are also required by most phytoplankton (Croft et al. 2005), and have been found to colimit (with Fe) Southern Ocean phytoplankton communities in austral summer along the WAP (Panzeca et al. 2006) and in the Ross Sea (Bertrand et al. 2007; Bertrand et al. 2011). Field studies have also identified exceedingly low concentrations of manganese (Mn) in surface waters of the ACC (Martin et al. 1990*b*; Middag et al. 2011; Hatta et al. 2013; Moore et al. 2013) and the Weddell Sea (Middag et al. 2013) in austral summer. Lab-based culture experiments have highlighted supply of both Fe and Mn as important drivers of productivity in Southern Ocean phytoplankton isolates of *Chaetoceros debilis* (Pausch et al. 2019) and *Phaeocystis antarctica* (Wu et al. 2019). Most recently, incubation experiments confirm that Fe, Mn, and Fe–Mn colimitation of phytoplankton communities all occur across the Drake Passage in austral spring (Browning et al. 2021). Spatial and temporal gradients in the bioavailability of Fe but also other trace metals and vitamins is, thus, expected to shape phytoplankton community composition in the Southern Ocean (Nolting and De Baar 1994; de Jong et al. 2012; Hatta et al. 2013; Viljoen et al. 2019).

In addition to gradients in total dissolved metal concentrations, trace metal bioavailability to phytoplankton is also influenced by changes in the chemical speciation (e.g., via organic complexation) of trace metals and competition between highly bioavailable free metal ions for cellular coordination sites (Brand et al. 1983; Sunda 1989). In the Southern Ocean, organic complexation of Cu by strong Cu-binding organic ligands leads to exceedingly low free, hydrated Cu^{2+} ion concentrations in austral winter surface waters of the ACC offshore and over the WAP shelf (Bundy et al. 2013). Similarly, gradients in the concentrations and organic complexation of Zn and Cd result in lower bioavailable inorganic Zn and Cd in surface waters of the Drake Passage in summer relative to deeper waters and surface waters approaching the WAP (Baars and Croot 2011; Baars et al. 2014). Phytoplankton growth in Southern Ocean waters may also lead to temporal changes in metal speciation and bioavailability via ligand production (Capodaglio et al. 1998; Buck et al. 2010) and via enhanced uptake of more abundant trace metal ions (e.g., Cd, Zn) in low Fe and Mn waters of the ACC (Cullen et al. 2003). Altogether, changes in dissolved concentrations and speciation of bioactive trace metals likely play an important role in phytoplankton community composition and productivity in this region that is otherwise macronutrient-rich (Martin et al. 1990*b*; Boyd et al. 2000; Viljoen et al. 2019).

Here, we investigate the interplay between trace metals, macronutrients, and phytoplankton growth in a series of three shipboard incubation experiments conducted using in situ Southern Ocean plankton assemblages. We used offshore ACC water from the Drake Passage and coastal Bransfield Strait water from the WAP to carry out experiments during early austral spring (September–October) 2016. The concentrations of dissolved Fe, Co, Mn, Ni, Cu, Zn, and Cd were measured over the course of the experiments along with macronutrients (nitrate + nitrite, soluble reactive phosphorus, silicic acid) and chlorophyll *a* (chl *a*) across control (unamended), +Fe, +vitamin B_{12}, +Fe-+vitamin B_{12}, and mixed inshore : offshore treatments. The results of this study highlight biogeochemical feedbacks between trace metal chemistry and phytoplankton growth across a range of initial trace metal conditions in the Southern Ocean, where trace metal chemistry and global ocean biogeochemistry are tightly coupled.

Methods

Incubation setup and sampling

Seawater from two locations was used for the three incubation experiments (Inc 1, Inc 2, Inc 3) conducted aboard the R/V/I/B *Nathaniel B. Palmer* in austral spring (Fig. 1a). A Sea-Bird GEOTRACES style SBE32 rosette system (Cutter and Bruland 2012) was deployed on a conducting Kevlar line with modified 12-L x-Niskin samplers (OceanTestEquipment, Inc.) to collect trace metal clean seawater from 25–35 m depth in September 2016.

The incubations were carried out in a temperature-controlled (3.5 ± 1.5°C, $n = 3405$) incubation van located in the ship's hold. For each incubation, unfiltered seawater from the x-Niskins was passed through an acid-cleaned 150-μm nylon mesh to remove any large grazers before it was homogenized in acid-cleaned 50-L polypropylene (PP) carboys (Fig. 1b). The seawater in the 50-L carboys was then evenly distributed into 4-L polycarbonate incubation bottles (Fig. 1b), which had been acid-cleaned, conditioned with Milli-Q water (≥ 18.2 MΩ cm), and rinsed with seawater following the same procedure as the carboys (Hollister et al. 2020). Each incubation bottle was given a unique number to track bottles across the experiments.

Incubation bottles were amended according to treatments chosen for each incubation (Fig. 1b). The stable isotope ^{57}Fe (as $^{57}FeCl_3$, Isoflex) was used for Fe amendments as a tracer. Eleven incubation bottles were filled for each incubation treatment, two of which were bagged in heavy duty black plastic bags for dark treatments and the remaining nine exposed to light conditions (Fig. 1b). The light bottles were exposed to continuous blue fluorescent light (108.1 ± 37.5 μmol photons m^{-2} s^{-1}, $n = 42$) as described previously (Hopkinson et al. 2007). Once all incubation bottles were filled and amended (*see* Fig. 1b for treatments), three to four incubation bottles from each treatment were sampled for the initial timepoints. Bottles were then sealed with parafilm around the outside of the caps to protect bottle threads, and secured with electrical tape.

Incubation bottles were gently inverted during the experiments to mix the contents. For each light-exposed treatment, three of the nine 4-L incubation bottles were sampled at

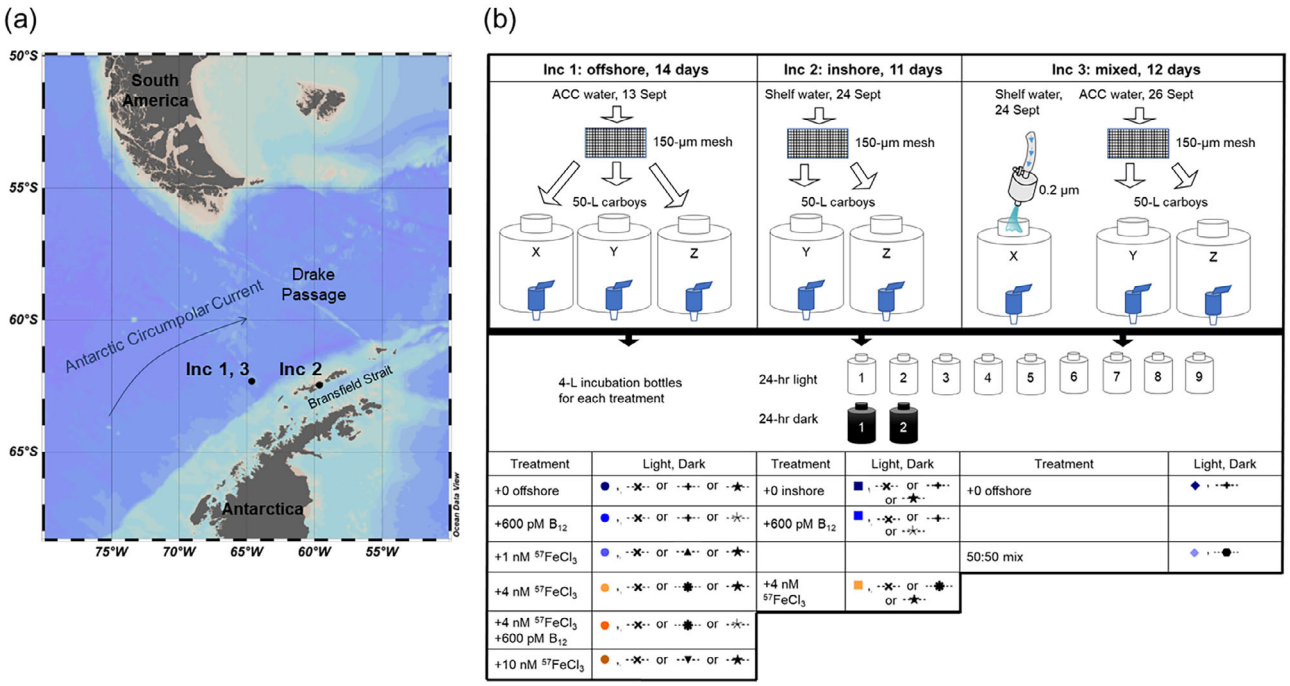

Fig. 1. (**a**) Locations (black dots) of surface seawater collection for shipboard incubations (Inc 1, Inc 2, Inc 3). Inc 3 water was collected at the same offshore location as Inc 1 (−62.33°N, −64.65°E) but included filtered (0.2 μm Acropak, pall) inshore water collected from the location of Inc 2 (−62.46°N, −59.57°E) as a "natural Fe" amendment in a 50:50 mixture [*see* (**b**)]. (**b**) Incubations setup and treatments. Symbols for the treatments are repeated in later figures. Shapes represent the incubation and colors correspond to the amount of Fe added.

random to yield three replicates per timepoint; additional treatment bottles were sampled on the final day. For dark treatments, one of the two 4-L incubation bottles per treatment was sampled per timepoint; both dark bottles were sampled for the final timepoints. The incubation bottles were repeat sampled over the course of each experiment, and cleaned with rinses of 10% HCl (TMG, Fisher), Milli-Q water, and incubation seawater between experiments. Incubation bottles were labeled by treatment to allow repeated use for those treatment conditions and to minimize carryover across incubation experiments.

Sampling and analyses

Chl a, *growth rate, lag phase*

Chl *a* samples were collected by vacuum filtration on 0.8 μm GF/F Whatman glass microfiber filters. The filters were leached with 95% ethanol immediately following collection and stored at room temperature in the dark for 12–24 h. Chl *a* concentrations were then determined from the extracts using a 10AU fluorometer (Turner Designs, Inc.) before and after acidification with 10% hydrochloric acid (Jesperson and Christoffersen 1987; Morison and Menden-Deuer 2015).

Growth rate (μ; d^{-1}) was determined over the incubation days (time) according to the equation (Wood et al. 2005):

$$\text{growth rate, } \mu = \frac{\ln(\text{final chl } a) - \ln(\text{initial chl } a)}{\text{time}}. \quad (1)$$

We defined the lag phase of our experiments by the time (in days) it took for the first significant change in chl *a* to occur ($p < 0.05$, *t*-test).

Dissolved macronutrients

Samples for dissolved nitrate + nitrite ("N+N"), soluble reactive phosphorus ("phosphate"), and silicic acid were filtered through sequential 3 and 0.4 μm polycarbonate track-etched (PCTE) filters (Whatman Nuclepore) on Teflon dual-stage filter rigs (Savillex) connected to a custom-made, trace-metal-clean vacuum filtration system. The filters were acid-cleaned with a 1-month soak in 10% TMG Fisher HCl, then Milli-Q rinsed and stored in pH 2 Milli-Q prior to use, allowing for collection of both dissolved trace metal and macronutrient samples from the same filtration setup. Macronutrient samples were collected in 50-mL conical PP tubes (Falcon) that had been soaked at least overnight in 10% HCl (Fisher, TMG), rinsed with Milli-Q three times and rinsed with filtered seawater sample prior to filling. Samples were stored in a refrigerator (4°C) until analyzed shipboard.

Samples were analyzed at sea within 24 h of collection on a Lachat 8500 QuickChem analyzer, and again back in the laboratory on a Seal Analytical Technicon AAII according to

standard methods (Parsons et al. 1984; Gordon et al. 1993). For each run, duplicate five-point standard curves and reagent blanks were run. Quality control (QC) sample checks were run every seventh sample. Filtered and autoclaved surface water collected from the ACC was used for the bulk seawater QC sample. To account for instrument drift, the midpoint of the calibration curve was analyzed every 14th sample.

Dissolved trace metals (Fe, Co, Mn, Ni, Cu, Zn, Cd)

Samples for dissolved trace metals were filtered by vacuum filtration as described for dissolved macronutrients above, and the filtrate (< 0.4 μm) was collected in 125-mL low-density polyethylene (LDPE) bottles. The 125-mL LDPE bottles were cleaned with 1% Citrad in RO water, rinsed with RO water, acid-cleaned with 25% nitric acid (HNO_3; Reagent Grade, Fisher) for 2 months, rinsed with Milli-Q water, stored filled with 0.1 mol L^{-1} HCl (TMG, Fisher), and rinsed three times with sample before filling. Upon collection, dissolved samples were acidified to pH < 1.8 (0.024 mol L^{-1} HCl; Optima, Fisher) (Johnson et al. 2007) and stored double-bagged at room temperature for several months prior to analysis at the University of South Florida.

All samples, including seawater standard curves, reference materials, and QC samples, were subjected to ultraviolet oxidation for 90 min in a UVO-Cleaner (Model No. 342; Jelight Company Inc.) (Hollister et al. 2020) to allow complete extraction of Co and Cu (Biller and Bruland 2012). Extraction and preconcentration of dissolved trace metals was then performed using an Elemental Scientific (ESI) seaFAST-pico system (Lagerström et al. 2013; Hollister et al. 2020). We adjusted the NH_4Ac buffer to pH 7.4 ± 0.2 and decreased the buffer flow rate in the submethod to 400–350 s-μL min^{-1} to conserve reagents (Jensen et al. 2020). Samples were buffered to a pH of 6.2 ± 0.3 to optimize recovery (Sohrin et al. 2008). The extracted trace metals were eluted with 5% HNO_3 (TMG, Fisher; triple-distilled using a Savillex DST-1000 Acid Purification System) with 10 ppb indium (In) internal standard (hereafter referred to as "elution acid") (Hollister et al. 2020) into 2.0-mL polyvinylidene fluoride vials (ESI) and capped with Teflon caps (ESI). Prior to initial use, new eluent vials and caps were soaked in a soap bath (1% Citrad in RO water), rinsed with RO water, heated in a 10% HCl (TMG, Fisher) bath, rinsed with Milli-Q water, heated in a 10% HNO_3 (TMG, Fisher) bath, and Milli-Q rinsed. In-between uses, caps and vials were re-cleaned in a heated 10% HNO_3 (TMG, Fisher) bath and Milli-Q rinsed.

Seawater calibration curves were made in filtered (< 0.2 μm, Pall Acropak) offshore ACC seawater collected from 25–35-m depth and stored unacidified in an acid-cleaned, seawater-rinsed 50-L PP carboy. Aliquots (2-L) were acidified to pH 1.8 (0.024 mol L^{-1}) with Optima (Fisher) HCl and used to prepare mixed metal standard curves by dilution of 1000 ppm Fe, Co, Mn, Ni, Cu, Zn, and Cd standards (Ultra Scientific). A standard curve of $^{57}FeCl_3$ (Isoflex) was also made. Each seawater calibration curve was comprised of a minimum of six points placed at the beginning and end of each seaFAST run. Each seaFAST run also included a series of reference samples (SAFe D2, GEOTRACES GS, GSC) and our own QC samples to assess analytical accuracy and precision (Table S1). Two QC samples were made, one from the same acidified ACC seawater used for the calibration curves and the second QC from homogenized and acidified offshore seawater collected in the Eastern Pacific (GEOTRACES cruise GP16) (Buck et al. 2018*b*). Reference and QC samples were run at least every 15 samples on the seaFAST.

SeaFAST eluents were analyzed on a Thermo Scientific magnetic sector Element XR High Resolution Inductively Coupled Plasma Mass Spectrophotometer (HR-ICP-MS) for ^{55}Mn, ^{56}Fe, ^{57}Fe, ^{59}Co, ^{60}Ni, ^{63}Cu, ^{65}Zn, molybdenum-95 (^{95}Mo), ^{111}Cd, and ^{115}In. The Element XR autosampler probe was rinsed twice with 5% HNO_3 (TMG, Fisher) between samples to avoid carryover. To account for any interference of MoO^+ on ^{111}Cd counts, a three-point Mo elution acid calibration curve was used to correct the ^{111}Cd counts in all samples. Natural abundance dissolved trace metal concentrations were calculated by dividing the ^{115}In-normalized counts for each sample by the ^{115}In-normalized seawater calibration curve slope of each trace metal. Any ^{56}Fe in the $^{57}FeCl_3$ spike was corrected for by using an $^{57}FeCl_3$ elution acid curve made separately from the natural abundance trace metal standards. For samples treated with $^{57}FeCl_3$, the concentration of ^{57}Fe added was calculated by subtracting natural abundance ^{57}Fe determined from a mixed metals elution acid curve. Air blanks, measured with a minimum of three replicates per seaFAST and Element XR run (Hollister et al. 2020), were subtracted from the dissolved sample concentrations. Limits of detection were calculated as three times the standard deviation of the air blanks (Table S1).

Results and discussion

Early austral spring conditions

We initiated our incubation experiments in mid-September around the austral spring equinox as daylight was rapidly increasing. In situ chl *a* concentrations were low at both of our study sites and increased over the course of the cruise (Sterling et al. 2022). Initial chl *a* concentrations in our incubations captured these environmental conditions, with lower initial chl *a* and longer lag times in Inc 1 (0.18 ± 0.05 μg L^{-1}, n = 18; 5 d lag) than observed in Inc 3 (0.52 ± 0.05 μg L^{-1}, n = 3; 3 d lag) at the same offshore location 2 weeks later (Fig. 2; Tables S2, S7). Initial chl *a* in Inc 2 (0.23 ± 0.03 μg L^{-1}, n = 9) was low as well, but lag time (3 d lag) was much shorter than the ~ 10-d lag reported for a similar incubation conducted in austral winter (July) in the same region of Bransfield Strait (Buck et al. 2010), consistent with the initiation of our incubations later in the year. Across all of our incubations and treatments, chl *a* concentrations increased upon exposure to continuous blue light in the shipboard incubation van (Fig. 2). Temperatures in our incubation van (3.5 ± 1.5°C,

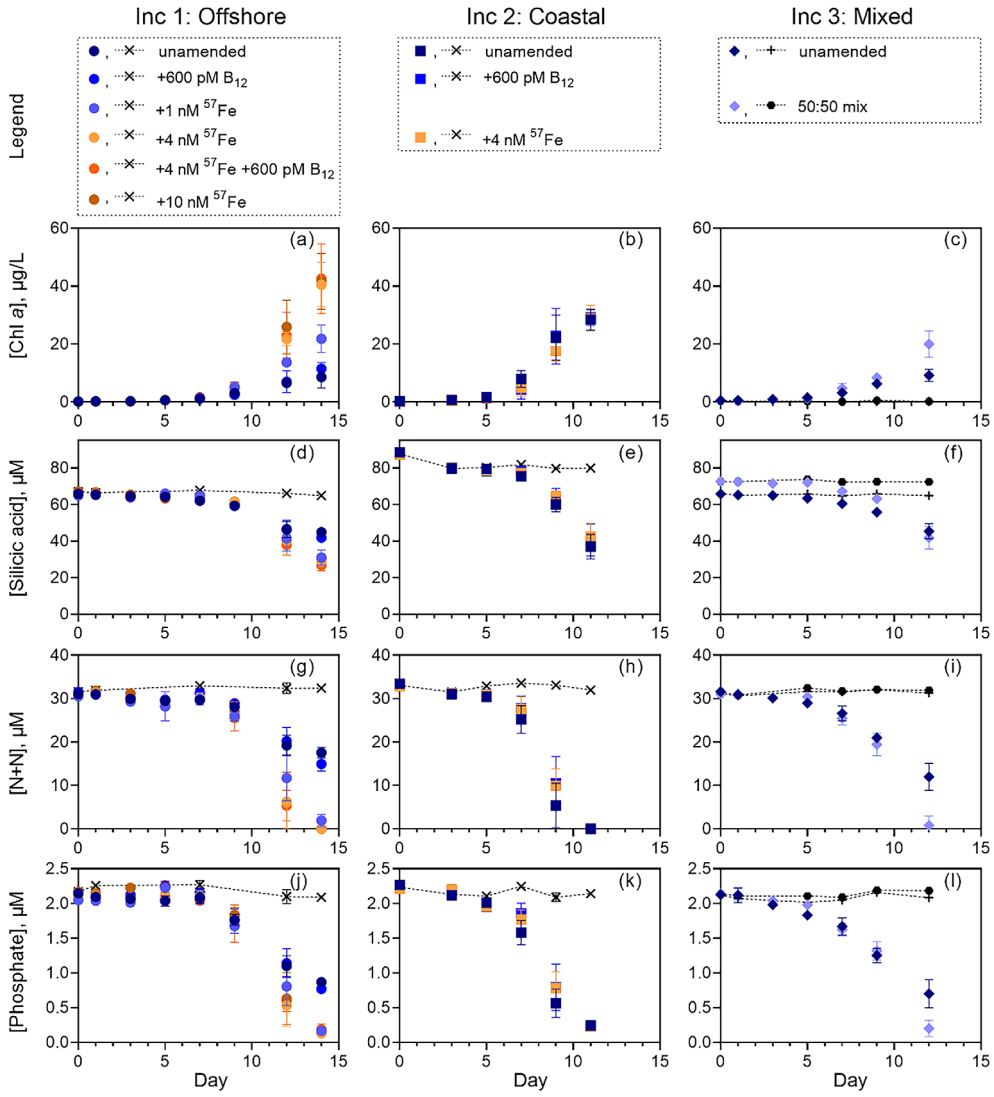

Fig. 2. Concentrations of chlorophyll *a* (chl *a*, in μg L^{-1}; **a–c**), and of dissolved (< 0.4 μm) silicic acid (in μmol L^{-1}; **d–f**), nitrite + nitrate (N+N, in μmol L^{-1}; **g–i**), and soluble reactive phosphorus (phosphate, in μmol L^{-1}; **j–l**) for incubations 1–3. Error bars are standard deviation of the replicate ($n \geq 3$) treatment bottles sampled at each timepoint. For bottles exposed to 24-h blue, fluorescent light, symbols correspond to average concentrations for each treatment. For bottles placed in 24-h darkness, symbols correspond to combined averages across treatments in each seawater matrix and are connected by dotted lines.

$n = 3405$) were also warmer than the in situ temperatures (-1.7 ± 0.1°C, $n = 220$). Phytoplankton growth in all treatments was, thus, stimulated by exposure to continuous light, and perhaps also by the warmer temperatures in the incubation van and by decoupling from large grazers in the incubation bottles.

Phytoplankton communities in both inshore and offshore experiments were dominated by diatoms (FlowCam data not shown) that clustered primarily by location of the incubation, with oceanic diatoms dominating all treatments of Inc 1 and Inc 3, and neritic diatoms dominating Inc 2 (18S rDNA sequencing data not shown). We also observed *Phaeocystis* colonies uniquely in the Inc 3 treatments (FlowCam data not shown). Phytoplankton uptake of dissolved trace metals relative to phosphate (ΔM:ΔP, in mmol mol^{-1}) was calculated from the difference in dissolved concentrations between the initial and final timepoints in each light treatment of each incubation (Table 1):

$$\Delta M{:}\Delta P = \frac{[M]_{final} - [M]_{initial}}{[P]_{final} - [P]_{initial}}. \quad (2)$$

Dissolved trace metal concentrations did not significantly differ between the carboys used for incubation setup (Table S3) and the unamended 4-L incubation bottles (Tables S4, S6, S8) ($p < 0.05$, *t*-tests). Initial concentrations

Table 1. Measured change (Δ) in dissolved metal (M) relative to soluble reactive phosphorus (P) for iron (Fe), cobalt (Co), manganese (Mn), nickel (Ni), copper (Cu), zinc (Zn), and cadmium (Cd), ΔFe:ΔMn, Δsilicic acid (Si):Δnitrate + nitrite (N), and growth rate over the course of the incubations for each treatment. The ΔM:ΔP and ΔFe:ΔMn were calculated according to Eq. 2 in the text. For ΔSi:ΔN, ratios were calculated between the initial and second-to-last sampling day ($T_{final-1}$) since N was drawn down to below detection on the final day. Growth rate was calculated according to Eq. 1 in the text. Error bars represent standard deviation of results from replicate incubation bottles, except for growth rate, where error bars are standard error. Results for ΔM:ΔP are compared against published values in the Southern Ocean.

Source	Treatment	ΔMn:ΔP mmol mol^{-1}	ΔFe:ΔP* mmol mol^{-1}	ΔCo:ΔP mmol mol^{-1}	ΔNi:ΔP mmol mol^{-1}	ΔCu:ΔP mmol mol^{-1}	ΔZn:ΔP mmol mol^{-1}	ΔCd:ΔP mmol mol^{-1}	ΔFe:ΔMn* mol mol^{-1}	ΔSi:ΔN mol mol^{-1}	Growth rate d^{-1}
Inc 1†, 14 d	+0 offshore	0.48±0.04	−0.13±−0.12	0.01±0.01	0.49±0.70	0.25±0.03	2.82±0.32	0.36±0.03	−0.28±−0.26	1.65±0.50	0.24±0.04
	+600 pmol L^{-1} B_{12}	0.42±0.02	−0.16±−0.16	0.01±0.03	0.51±0.52	0.28±0.04	2.66±0.35	0.33±0.02	−0.38±−0.38	1.77±0.66	0.30±0.04
	+1 nmol L^{-1} $^{57}FeCl_3$	0.35±0.02	0.39±0.08	0.01±0.01	0.49±0.43	0.27±0.02	2.31±0.27	0.30±0.02	1.13±0.24	1.25±0.51	0.31±0.03
	+4 nmol L^{-1} $^{57}FeCl_3$	0.35±0.02	1.69±0.16	0.01±0.00	0.56±0.29	0.27±0.02	2.35±0.20	0.32±0.02	4.77±0.50	1.02±0.42	0.37±0.03
	+600 pmol L^{-1} B_{12} + 4 nmol L^{-1} $^{57}FeCl_3$	0.31±0.03	1.07±0.07	0.04±0.02	0.55±0.39	0.26±0.03	2.07±0.15	0.28±0.03	3.46±0.35	1.10±0.27	0.37±0.05
	+10 nmol L^{-1} $^{57}FeCl_3$	0.33±0.02	3.58±0.13	0.02±0.00	0.61±0.38	0.24±0.02	2.14±0.17	0.30±0.02	10.94±0.64	1.08±0.43	0.35±0.04
Inc 2†, 11 d	+0 inshore	1.98±0.10	2.04±0.56	0.03±0.01	0.66±0.27	0.28±0.08	2.20±0.38	0.30±0.04	1.03±0.29	1.02±0.23	0.32±0.05
	+600 pmol L^{-1} B_{12}	1.89±0.10	1.58±0.83	0.07±0.03	0.42±0.16	0.20±0.07	2.16±0.17	0.27±0.02	0.84±0.44	1.11±0.42	0.34±0.06
	+4 nmol L^{-1} $^{57}FeCl_3$	2.00±0.11	3.33±0.56	0.03±0.00	0.54±0.16	0.20±0.07	2.61±0.30	0.30±0.03	1.66±0.29	0.99±0.21	0.40±0.04
Inc 3†, 12 d	+0 offshore	0.45±0.09	−0.14±−0.16	0.02±0.01	0.49±0.32	0.23±0.09	2.97±0.58	0.35±0.08	−0.31±−0.36	0.94±0.15	0.19±0.02
	50:50 mix offshore: filtered inshore	1.13±0.14	0.41±0.18	0.02±0.01	0.42±0.28	0.27±0.08	2.11±0.26	0.29±0.03	0.36±0.16	0.82±0.25	0.28±0.03
Twining and Baines (2013)	Southern Ocean (diatoms)‡	1.7	–	0.15	1.68	1.44–2.00	11.10–13.30	0.07–1.29			
	Southern Ocean§	–	0.20±0.04	0.041±0.005	1.80±0.10	0.53±0.13	6.0±2.6	0.65±0.30			
Cullen et al. (2003)†, 11 d	+0	0.61	–	0.29	–	0.51	3.96	0.62			
	+1 nmol L^{-1} Fe (natural abundance)	0.70	–	0.10	–	0.60	2.91	0.44			
Buck et al. (2010)†, 15 d	+0	–	3.42±0.21	–	–	0.36±0.13	–	–			
	+0.9 nmol L^{-1} $^{57}FeCl_3$	–	3.23±0.15	–	–	0.28±0.10	–	–			
Janssen et al. (2020)	Mertz glacier polynya‖	–	–	–	1.34±0.24	0.69±0.10	3.11±0.41	0.53±0.07			
	Amundsen Sea¶	–	–	–	0.29	0.69	3.37	–			
Viljoen et al. (2019)#	Weddell gyre	0.116–0.167	0.05–0.50	−0.199-0.00245	0.80–1.86	0.96–1.93	5.37–6.87	0.323–0.661			
	Antarctic zone	0.11–0.156	0.22–0.43	−0.00051-0.00812	1.09–1.28	0.60–0.79	4.39–5.35	0.552–0.667			
	Polar frontal zone	−0.04	0.54	−0.0104	1.77	1.44	5.26	0.591			
Bown et al. (2017)#	Ryder Bay, Antarctic Peninsula	1.45–1.89	1.10–1.76	0.0076–0.0190	–	0.29–0.71	0.222–0.270	2.03–2.49			

*Includes ambient Fe plus any ^{57}Fe added.
†Calculated as change in dissolved concentrations in the light over the full length of incubation.
‡Data from bulk environmental particulate samples from Collier and Edmond (1984) and Cullen et al. (2003).
§Data from regressions of dissolved concentrations from studies compiled by Twining and Baines (2013).
‖Data are inferred biological uptake from surface waters.
¶Data calculated from dissolved profiles in Sherrell et al. (2015).
#Data calculated from dissolved profiles.

from the 4-L incubation bottles were used for the calculations of metal uptake and for the remaining discussion.

The concentrations of macronutrients and trace metals in our incubation waters, collected from 25–35-m depth, were generally high and more consistent with much deeper waters (300–400 m) sampled in summer (Martin et al. 1990*b*). Thus, initial nutrient conditions were consistent with early spring initiation, prior to substantial phytoplankton growth, when surface waters still held the characteristics of winter mixing. Concentrations of macronutrients and most trace metals (Mn, Fe, Co, Cu, Zn; not Ni, Cd) were also significantly higher inshore than offshore (Figs. 2–4; Table S2, S4–S8). This inshore–offshore concentration gradient led to distinct initial conditions between the experiments, especially for silicic acid, Fe, Mn, and Co (Figs. 2–4).

Dissolved macronutrient and trace metal concentrations declined as biomass increased in the incubations (Figs. 2–4). Across the three experiments, near-complete N+N depletion was achieved by the final day in the high Fe Inc 1 treatments ($> +1$ nmol L^{-1} $^{57}FeCl_3$ added), all Inc 2 treatments, and the Inc 3 50:50 mix treatment (Fig. 2; Table S2, S5, S7). Phosphate was drawn down by $\sim 90\%$ on the final day in these same treatments (Fig. 2; Table S2, S5, S7). In the unamended offshore incubations, substantial drawdown of N+N and phosphate was also observed, but residual concentrations of both remained at the last timepoint (~ 10 μmol L^{-1} N+N, ~ 1 μmol L^{-1} phosphate; Fig. 2). Initial silicic acid concentrations were very high, more than double N+N concentrations, in both inshore and offshore experiments (Fig. 2, Table S2, S5, S7). Additions of Fe to the offshore incubations led to lower ratios of Si:N+N drawdown, with ΔSi:ΔN approaching 1 in inshore and Fe-amended treatments (Fig. S1; Table 1).

Iron

Iron was the primary limiting nutrient in the offshore ACC incubation waters (Inc 1 and 3). Initial Fe:N+N in Inc 1 and 3 were very low, < 0.02 nmol:μmol (Table S9), and Fe additions resulted in a significant ($p < 0.05$, *t*-test) increase in chl *a* biomass, higher growth rates, and macronutrient depletion in the light compared to the treatments with no Fe added (Fig. 2; Table 1, S2, S7). In the $+1$ nmol L^{-1} $^{57}FeCl_3$ treatment of Inc 1 (initial Fe:N+N $= 0.035 \pm 0.004$ nmol:μmol), roughly 2 μmol L^{-1} N+N remained at the end of the experiment. In Inc 1, treatments with $\geq +4$ nmol L^{-1} $^{57}FeCl_3$ achieved significantly ($p < 0.05$, t-test) higher final chl *a*, 41.5 ± 8.6 μg L^{-1} ($n = 9$) than any of the other treatments and were the only Inc 1 treatments where N+N was drawn down to near or below detection limits by the last day of the incubation (Fig. 2). Initial Fe:N+N following the $\geq +4$ nmol L^{-1} $^{57}FeCl_3$ additions in Inc 1 ranged from 0.11 to 0.27 nmol:μmol (Table S9). In our second offshore incubation, Inc 3, initial Fe concentrations were higher than Inc 1 and the 50:50 mix treatment of Inc 3 that added ~ 1 nmol L^{-1} Fe from inshore waters (initial Fe:N+N $= 0.054 \pm 0.010$ nmol:μmol) led to complete N+N drawdown. Thus, our results suggest that offshore waters with initial Fe:N+N below 0.05 nmol:μmol were Fe-limited, which is consistent with previous work in the ACC (Martin et al. 1990*b*) (Table S9).

The inshore waters of Bransfield Strait used for Inc 2, on the other hand, were Fe-replete. Final chl *a* and macronutrient concentrations in Inc 2 were indistinguishable between $+4$ nmol L^{-1} $^{57}FeCl_3$ and treatments with no added Fe (Fig. 2, Table S5). Initial Fe:N+N averaged 0.203 ± 0.027 nmol:μmol in the unamended Inc 2 treatment (Table S9) and N+N was depleted to below detection limits by day final in all treatments (Fig. 2; Table S5). In an austral winter study at the same location, slightly lower initial Fe and Fe:N+N (0.16 nmol:μmol) were observed, along with a strong chl *a* response to a ~ 1 nmol L^{-1} $^{57}FeCl_3$ addition that suggested Fe limitation (Buck et al. 2010). Our findings of Fe-replete conditions over the WAP shelf in early spring are more consistent with previous studies conducted in summer (Martin et al. 1990*b*; Helbling et al. 1991; Hopkinson et al. 2007). However, differences in initial conditions between Inc 2 and the austral winter incubation of Buck et al. (2010) were small and suggest that relatively minor changes in the supply of Fe can lead to Fe-limiting conditions even over the WAP shelf.

During the lag phase of our experiments, prior to significant changes in chl *a* biomass, dissolved M:P were constant for all metals except Fe, Mn, and Zn (Figs. S2, S3). For Fe, a strong decline in Fe:P was observed during this lag time as Fe, and especially added $^{57}FeCl_3$, was preferentially removed (Figs. 3, S2). This early drawdown of Fe in the light was greater than the Fe decline in the dark (Fig. 3) and was observed across all three incubations, consistent with luxury uptake of Fe by both inshore and offshore diatom communities prior to growth (Sunda and Huntsman 1995).

In the dark, Fe concentrations showed lower but still dramatic declines, especially in the treatments with added $^{57}FeCl_3$ (Fig. 3). This loss in the dark likely represented abiotic loss of Fe to the walls of the incubation bottles (Table S10) and precipitation of $^{57}FeCl_3$ added in excess of ambient Fe-binding organic ligands. We used a 150-μm prefilter to remove large grazers (Fig. 1b) but particles were not otherwise excluded from our experiments by design. Thus, it is plausible that some of the Fe decline in the dark resulted from scavenging onto particles or microbial uptake, though the consistency of our dark Fe losses (Table S11) with previous studies (Fischer et al. 2007; Buck et al. 2010; Fitzsimmons and Boyle 2012; Mellett et al. 2018) and the lack of P uptake in the dark (Fig. 2) suggest this loss of Fe in the dark was primarily abiotic (*see* additional discussion in Supporting Information).

A surprising finding from our experiments was that dissolved Fe inventories were never fully depleted, even in the Fe-limited waters offshore. This suggests that some portion of the dissolved Fe pool was not bioavailable, and/or that Fe was being efficiently recycled. We saw evidence for regeneration of dissolved Fe following N+N exhaustion in our incubation of

Fe-replete inshore waters (Inc 2, Fig. 3). Dissolved Fe concentrations in the offshore Inc 1 and Inc 3 treatments with no added Fe were similar between initial and final timepoints (Fig. 3) despite ~10 μg L^{-1} biomass increase and substantial macronutrient drawdown (Fig. 2). Consequently, phytoplankton nutrient quotas calculated from changes in the dissolved inventories concluded no Fe demand and even a net loss of Fe by phytoplankton growing in unamended offshore treatments (i.e., ΔFe:ΔP < 0 mmol mol^{-1}) (Fig. 5; Table 1). It is possible that contamination during the setup and sampling of the incubations contributed background Fe to the incubations, though we also note good agreement between replicate incubation bottles of the unamended treatments (Fig. 3) which were a mix of independent incubation bottles each sampling. Alternatively, our results suggest that Fe already in the biogenic particulate phase (i.e., not measured as dissolved Fe in the initial bottles) was efficiently recycled to support the observed growth. Previous work has identified the importance of recycled Fe to balance Fe supply and demand in open ocean surface waters of the Southern Ocean waters (de Jong et al. 2012), which is also supported by recent Fe isotope data in the ACC (Sieber et al. 2021). In general, efficient Fe recycling may be an important adaptation for phytoplankton growth in Fe-limited high-nutrient low-chlorophyll regions (Rafter et al. 2017).

Manganese

After Fe, the trace element most likely to serially limit phytoplankton growth in our incubations was Mn, which has been shown to limit and colimit phytoplankton in central Drake Passage in austral spring (Browning et al. 2021). In our offshore incubations, initial dissolved Mn concentrations were higher than dissolved Fe, but were also depleted before N+N in the treatments with added Fe (Figs. 2, 4). Our measured dissolved Mn:P ratios in Inc 1 diverged following the onset of phytoplankton growth (Fig. S3), declining in treatments with no added Fe and increasing in treatments with added Fe. As a result, Inc 1 exhibited growth rate dilution of ΔMn:ΔP, with higher Mn:P uptake under Fe-limiting conditions and declining ΔMn:ΔP with increasing Fe and higher resulting growth rates (Fig. S4; Table 1).

Inshore waters used for Inc 2 and the 50:50 mix of Inc 3 were Fe-replete and rich in Mn, with inshore Mn concentrations ~six-fold higher than in the offshore waters. Nevertheless, Mn:P uptake (ΔMn:ΔP) was also much higher in these waters (Figs. 5, S5; Table 1). In fact, across our experiments, ΔMn:ΔP was tightly coupled to initial dissolved Mn:P (Fig. 5), but not to initial Fe (Fig. S1).

Another intriguing feature in our Mn data was the absence of Mn drawdown in the dark. Previous dark incubations (Mellett et al. 2018) and remineralization experiments (Cheize et al. 2019; Hollister et al. 2020) have shown pronounced declines in dissolved Mn due to Mn oxidation, which rivaled Mn drawdown observed in matching light bottles (Mellett et al. 2018). However, despite the presence of bacteria genera in our incubation bottles capable of oxidizing Mn (*Acinetobacter*, *Sulfitobacter*; 16S rDNA sequencing data not shown) in Inc 1, warmer temperatures in our incubation van relative to in situ (*see* above), and the incubation of inshore waters that were highly enriched in dissolved Mn (Fig. 4), Mn decline in the dark was minimal across our experiments. Previous studies have also reported an apparent lack of Mn oxidation in the Southern Ocean, evinced by the absence of Co scavenging (Saito et al. 2010) and of Mn(IV) particulate phases (Oldham et al. 2021). Given the role of Mn oxides in scavenging Fe and other trace metals during regeneration (Cheize et al. 2019; Hollister et al. 2020), a lack of Mn oxidation may be an important contributor to recycling of Fe and other bioactive metals that would otherwise be scavenged onto particulate Mn oxides.

Cobalt

The addition of vitamin B_{12} in our incubations, whether with or without +4 nmol L^{-1} $^{57}FeCl_3$ offshore (Inc 1) or in naturally Fe-replete waters inshore (Inc 2), led to similar final concentrations of chl *a*, macronutrients, and most trace metals as measured in equivalent Fe treatments with no vitamin B_{12}. Addition of just vitamin B_{12} to Inc 1 offshore led to a 10-fold increase in measured initial dissolved Co:P but did not result in higher ΔCo:ΔP (Fig. 5), which implies that vitamin B_{12} was not a preferred form of Co for the Fe-limited offshore communities. We did not measure vitamin B_{12} in our experiments, but our results suggest that natural vitamin B_{12} concentrations were sufficient to support the phytoplankton growth observed.

In the absence of vitamin B_{12} additions, a positive relationship between initial dissolved Co:P and Co:P uptake (ΔCo:ΔP) was observed across all three incubations, including inshore and offshore diatom communities, and Fe-limited and Fe-replete waters (Fig. 5). Thus, total Co:P uptake in our experiments was largely independent of initial Fe and growth rate (Figs. S1, S4). Over the course of our experiments, dissolved Co concentrations encompassed the seasonal range reported in surface waters of the Ross Sea (Saito et al. 2010), with initial concentrations matching austral spring ranges and final concentrations in the Fe-replete and Fe-amended incubations approaching the lowest summer values (20–30 pmol L^{-1}; Tables S4, S6, S8). These results suggest that ambient dissolved Co in the incubation waters inshore and offshore were bioavailable, although drawdown of dissolved Co was initiated later in the experiments than Mn, Zn, or Cd (Figs. 3, 4).

The development of Fe-vitamin B_{12} colimiting conditions reported along the WAP in austral summer (Panzeca et al. 2006) may reflect seasonal cycles in vitamin B_{12} inventories (Sañudo-Wilhelmy et al. 2006). Addition of vitamin B_{12} with 4 nmol L^{-1} $^{57}FeCl_3$ to Inc 1, and alone to the naturally Fe-replete waters of Inc 2, led to higher ΔCo:ΔP than in the

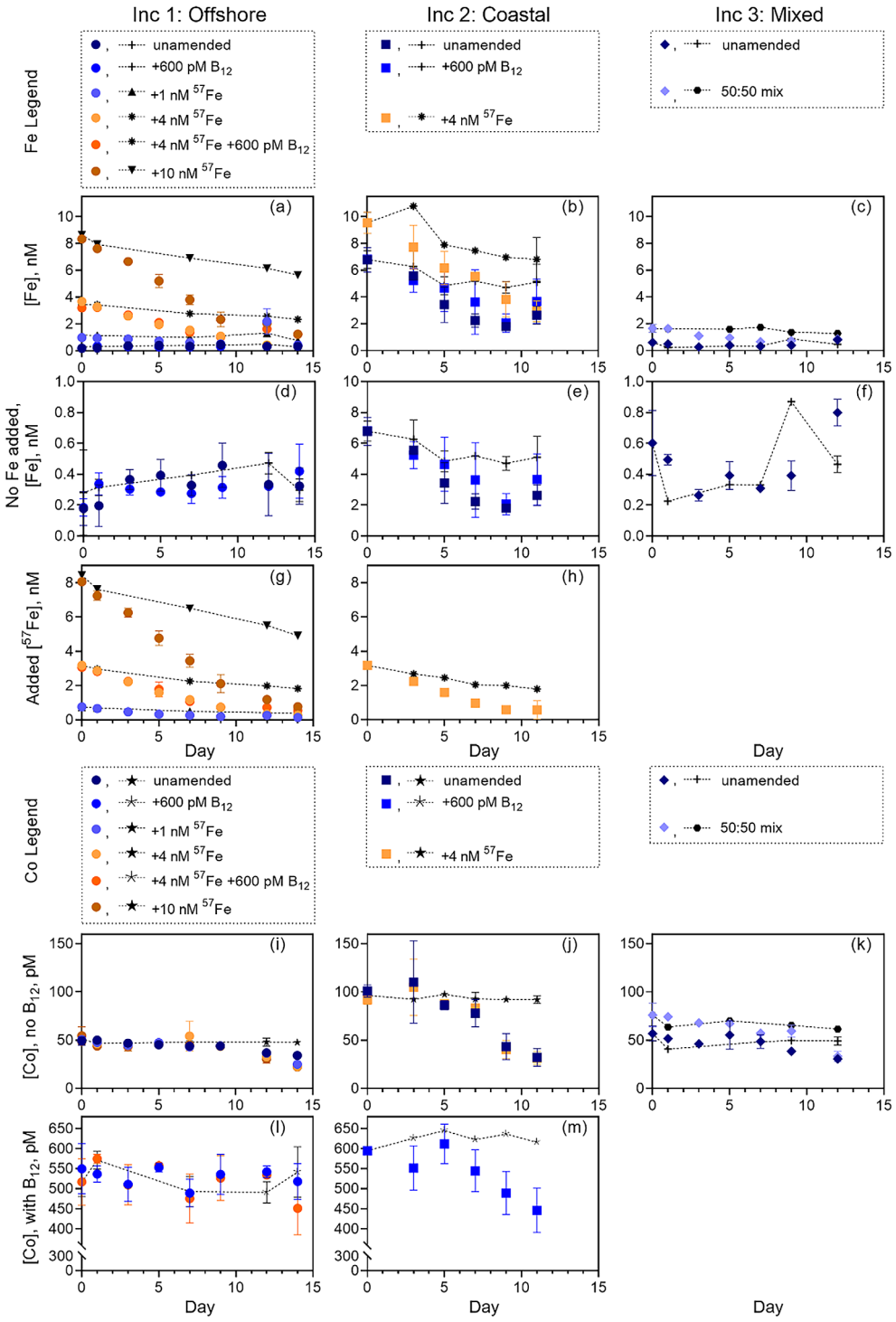

Fig. 3. Dissolved (< 0.4 μm) iron (Fe; **a–h**) and cobalt (Co; **i–m**) concentrations for incubations 1–3 (Inc 1–3). Dissolved Fe is presented as total dissolved Fe (**a–c**) and includes both natural dissolved Fe in the seawater and any ^{57}Fe added as a treatment. Dissolved Fe in treatments with no Fe addition (**d–f**) and as added ^{57}Fe (**g**, **h**) are also presented. Dissolved Co results are presented separately for treatments without (**i–k**) and with (**l**, **m**) amendments of vitamin B_{12}, a Co-containing compound. Error bars represent standard deviations of results from replicate ($n \geq 3$) treatment bottles sampled at each timepoint. For bottles kept in dark, symbols correspond to averages combined from across treatments in each seawater matrix and are connected by dotted lines.

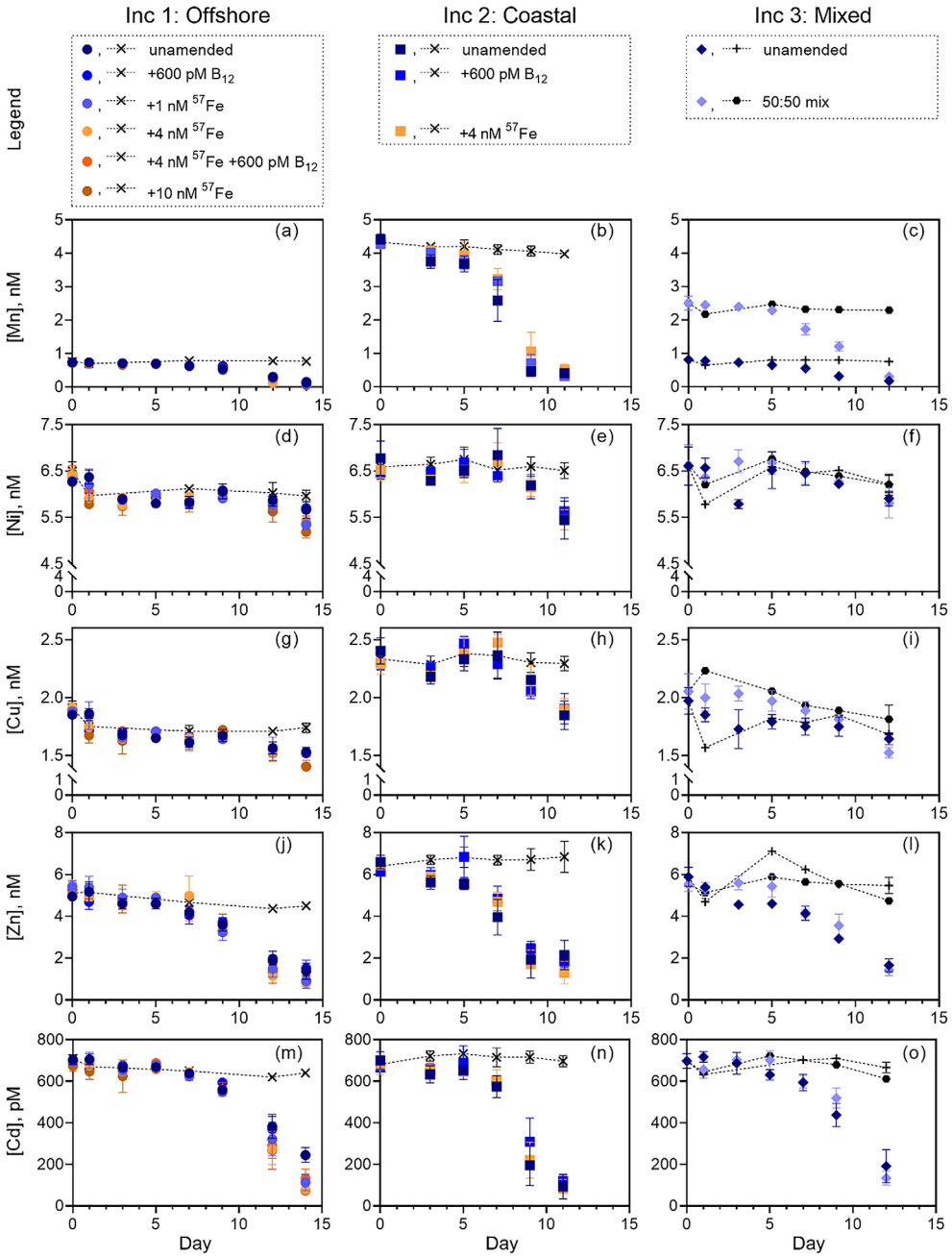

Fig. 4. Dissolved (< 0.4 μm) manganese (Mn; **a–c**), nickel (Ni; **d–f**), copper (Cu; **g–i**), zinc (Zn; **j–l**), and cadmium (Cd; **m–o**) concentrations for incubations 1–3 (Inc 1–3). Error bars represent standard deviations of results from replicate ($n \geq 3$) treatment bottles sampled at each timepoint. For bottles kept in dark, symbols correspond to averages combined from across treatments in each seawater matrix and are connected by dotted lines.

equivalent Fe treatments without vitamin B_{12} additions (Fig. 5; Table 1). The drawdown of dissolved Co (ΔCo) in the vitamin B_{12}-amended Fe-replete treatments was greater than the total background dissolved Co pool present before the vitamin B_{12} additions, indicating that some of the increase in ΔCo:ΔP was derived from taking up added vitamin B_{12} (Tables S4, S6). Thus, although the addition of vitamin B_{12} to Fe-replete incubations did not translate into significant increases in final chl *a* or macronutrient drawdown (Fig. 2; Tables S2, S5), the apparent acquisition of added vitamin B_{12} and resulting higher ΔCo:ΔP suggest that natural vitamin B_{12} sources in these treatments had been depleted.

Zinc

Initial dissolved Zn:P (Fig. S3) and Zn:Si ratios (Figs. S5, S6) were similar across the three experiments, consistent with

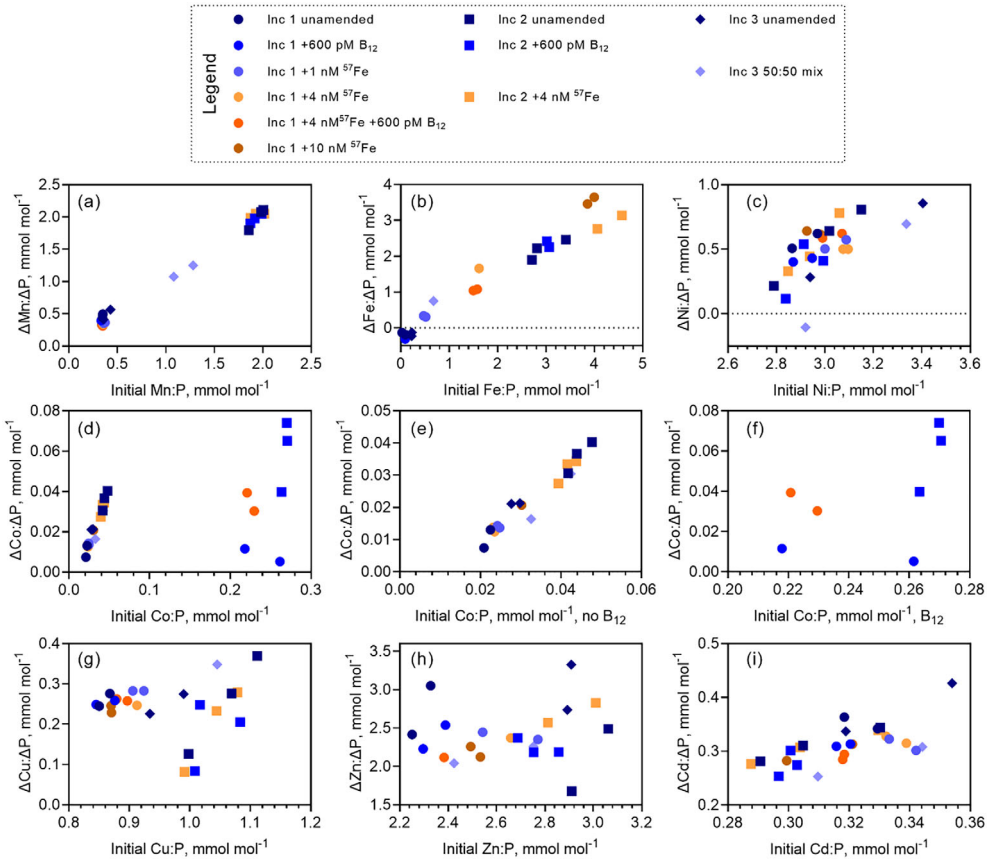

Fig. 5. Calculated uptake of dissolved (< 0.4 μm) trace metal concentrations relative to uptake of soluble reactive phosphorus (Δmetal:ΔP, *see* Eq. 2) plotted as a function of initial dissolved metal concentrations normalized to initial P in incubations 1–3 (Inc 1–3). Dissolved Fe is presented as total dissolved Fe and includes both natural dissolved Fe in the seawater and any ^{57}Fe added as a treatment. Delta values are calculated as the change in concentration between initial and final timepoints sampled in individual light bottles. Symbol colors correspond to Fe addition, and shapes correspond to incubation.

upwelling sources of Zn and macronutrients in Drake Passage and the WAP (Croot et al. 2011). We observed rapid drawdown of dissolved Zn in all three incubations. The highest Zn:P uptake (ΔZn:ΔP) was observed in the Fe-limited treatments offshore with no B_{12} added (Fig. 5; Table 1), and in these treatments, dissolved Zn:P decreased over the course of the incubations as Zn was preferentially removed relative to P (Fig. S3). Growth rate dilution (Cullen et al. 2003) of Zn uptake was observed offshore (Fig. S4; Table 1), resulting in much higher final dissolved Zn:P (Fig. S3).

Dissolved Zn and silicic acid (Si) tend to be tightly coupled in the ocean (Bruland 1980). In our experiments, initial dissolved Zn:Si ratios were relatively high (0.078 ± 0.005, $n = 11$), and Zn was preferentially drawn down relative to Si across all experiments and treatments leading to final Zn:Si (0.036 ± 0.009, $n = 11$) that were closer to measured Zn:Si in summer (Fig. S6) (Martin et al. 1990*b*; Croot et al. 2011). Notably, despite different initial Zn concentrations and very different growth responses across treatments, final dissolved Zn concentrations were remarkably similar at the end of the three incubations (Fig. 4; Tables S4, S6, S8) and Zn drawdown became decoupled from P and Si in Fe-replete waters inshore and offshore (Figs. 2, 4).

We observed plateauing dissolved Zn concentrations between the last two timepoints in Inc 1 and Inc 2, while other trace metals and macronutrient concentrations continued to decline and chl *a* was still increasing. It is possible that the early and rapid drawdown of Zn was sufficient to support the observed growth, particularly in Inc 1 where growth rate dilution of ΔZn:ΔP occurred with Fe additions (Fig. S4). In the Fe-replete incubations inshore and the high Fe treatments offshore, however, the lack of continued Zn drawdown with the other nutrients suggests that the bioavailability of the 1–2 nmol L^{-1} (average final [Zn], all light treatments, all incubations $= 1.52 \pm 0.56$, $n = 55$) remaining dissolved Zn was low, and that any remaining Zn demand was filled by either regenerated biogenic Zn or substitution for Zn by Cd or Co (Price and Morel 1990). We also found that additions of Fe decreased ΔZn:ΔP in offshore waters, consistent with growth rate dilution, but increased ΔZn:ΔP in inshore waters; in both settings dissolved Zn was rapidly drawn down to a similar apparent threshold.

Previous measurements of dissolved Zn speciation in the ACC and WAP region reported lower dissolved Zn and bioavailable inorganic Zn (Zn′) concentrations in summer surface waters, which increased with depth in the water column (Baars and Croot 2011). As described above, initial trace metal and macronutrient concentrations in our incubations in general were most consistent with subsurface (300–400 m) summer waters that had been upwelled over the winter and not yet drawn down by spring phytoplankton growth prior to our use in the incubations. If we use the speciation profile of Zn to match initial dissolved Zn concentrations at depth in south Drake Passage, the measured Zn′ concentrations at the same depth reported by Baars and Croot (2011) are similar to the total measured drawdown of Zn ($\Delta Zn = 4.13 \pm 0.33$ nmol L^{-1}, $n = 8$ treatments across Inc 1, 3; Tables S4, S8) in our experiments. Thus, the rapid drawdown of dissolved Zn observed in our incubations may have reflected the complete drawdown of bioavailable Zn′ in the initial waters, and the residual dissolved Zn that persisted even with continued growth in Fe-replete treatments may have been comprised of less bioavailable organically complexed Zn (ZnL).

Cadmium

Like Zn, dissolved Cd was rapidly depleted with phytoplankton growth in the experiments, though Cd drawdown appeared to start slightly later in the incubation period than Zn and continued after Zn drawdown plateaued in Inc 1 and Inc 2 (Fig. 4). Using the Cd* calculation introduced by Baars et al. (2014) for the Southern Ocean, our initial conditions were near 0 for all treatments (Fig. S7), consistent with recent upwelling of deeper waters. Organic complexation of Cd was also found to be less extensive for Cd than Zn in southern Drake Passage in summer (Baars et al. 2014), supporting our observations of high Cd bioavailability throughout the incubation experiments.

Dissolved Cd:P ratios were relatively constant over the course of the Fe-limited offshore incubations (Fig. S3). In the offshore treatments with Fe added, either as $^{57}FeCl_3$ (Inc 1) or natural Fe (Inc 3 50:50 mix), dissolved Cd:P increased during phytoplankton growth, and final dissolved Cd:P in the Fe-amended offshore treatments were nearly double initial Cd:P as P was preferentially depleted to support the enhanced growth rates (Fig. S4). This growth rate dilution of ΔCd:ΔP (Fig. S4), with higher uptake of Cd in Fe-limited waters offshore (Table 1), was similar to our observations of Zn:P and to previous reports of Cd:P and Zn:P in a Southern Ocean incubation (Cullen et al. 2003). Our results also suggest that ΔCd:ΔP was more dependent upon initial Cd:P at least across the relatively narrow range of initial Cd:P in our experiments (Fig. 5). This was not observed for Zn in our experiments (Fig. 5) or in the near-surface water incubations of Cullen et al. (2003), though our experiments were conducted in austral spring with higher initial Cd:P than the austral summer Cullen et al. (2003) incubations. Our initial Cd:P was more similar to deeper waters in summer profiles (Martin et al. 1990*b*; Baars et al. 2014).

Inshore, all treatments of Inc 2 were Fe replete, and both the unamended and + 4 nmol L^{-1} $^{57}FeCl_3$ treatment had relatively constant dissolved Cd:P over time (Fig. S3). So even though the growth rates and ultimate ΔCd:ΔP were similar between the offshore Fe-amended treatments and the naturally Fe-replete inshore treatments (Table 1), growth inshore did not lead to distinctly different dissolved Cd:P from initial Cd:P (Fig. S3). The exception to this was the Inc 2 +vitamin B_{12} treatment, which had an average growth rate between the unamended and +4 nmol L^{-1} $^{57}FeCl_3$ treatments, but lower apparent ΔCd:ΔP (Table 1) and a clear increase in dissolved Cd:P by the end of the incubation (Fig. S3). Thus, the addition of vitamin B_{12} to Inc 2, which led to the highest ΔCo:ΔP (Table 1), may have offset Cd demand in these communities.

Nickel

Diatoms typically have higher Ni requirements compared to other phytoplankton groups, and play a large role in Ni cycling (Twining et al. 2012). However, of the trace metals we measured, dissolved Ni exhibited the lowest percentage decline in the light bottles across the three incubations (Table S11). Average ΔNi:ΔP were similar across all treatments (Table 1), with relatively high variance between incubation bottles that appeared to be driven largely by inter-bottle differences in initial Ni:P (Fig. 5). We are not sure why the Ni concentrations varied between incubation bottles in a given treatment, but these differences occurred during incubation setup since they led to corresponding differences in total ΔNi:ΔP over the course of the incubations (Fig. 5). Previous studies have also reported high and variable Ni concentrations in the southern ACC (Nolting and De Baar 1994; Löscher 1999), with higher horizontal rather than vertical gradients in Ni profiles across the ACC.

The combination of low overall Ni percent decline in the light and a high responsiveness of ΔNi:ΔP to measured differences in initial Ni:P suggests low bioavailability of ambient dissolved Ni in these waters. In fact, ΔNi:ΔP may be overestimated in our offshore incubations, especially Inc 1, which showed a substantial decline in Ni and Cu at the onset of the experiment prior to a chl *a* response, perhaps reflecting scavenging to Fe oxyhydroxides precipitated from the inorganic Fe additions (Fig. 4). In all of our incubation treatments, dissolved Ni:P increased during phytoplankton growth as P was taken up preferentially relative to the initial conditions (Fig. S3). In the unamended inshore waters of Inc 2, more dissolved Ni was drawn down (ΔNi; Fig. 4) than in offshore waters, suggesting a gradient in Ni bioavailability between ACC surface waters and waters over the WAP shelf.

Our measured declines in Ni:P and Ni:Si (Figs. S3, S5, S6) were overall similar to calculated ratios for diatom cells and frustules, respectively (Twining et al. 2012), though our ΔNi:ΔP measurements encompassed both and were not parsed out

between organic matter and frustules, indicating less Ni drawdown than expected for diatoms. Meridional studies of trace metals have also suggested limited biological Ni uptake in ACC surface waters (Nolting and De Baar 1994; Löscher 1999; Viljoen et al. 2019). Recent Ni isotope measurements from the South Atlantic and Southern Ocean support limited dissolved Ni bioavailability to diatoms south of the Polar Front (Archer et al. 2020). Organic complexation of Ni may thus be an important contributor to Ni cycling in these waters, although we are not aware of any Ni speciation data from the Southern Ocean to date.

Copper

Previous studies have highlighted the similarities in dissolved Cu and Ni distributions in the southern ACC (Löscher 1999; Viljoen et al. 2019). Like Ni, relatively little Cu was drawn down across our experiments in the light (Table S11), more dissolved Cu was drawn down from unamended inshore waters relative to ACC waters offshore (Fig. 4), and dissolved Cu:P increased over time in all treatments of all incubations as P was drawn down preferentially with growth (Fig. S3). A previous Cu speciation study reported weaker organic complexation of Cu and higher resulting bioavailable Cu^{2+} concentrations in inshore waters compared to offshore waters in our study area in winter (Bundy et al. 2013), which could explain the higher apparent uptake of Cu relative to P in the incubation treatments that employed inshore waters.

Of all the elements we studied, Cu was the only trace metal to show very different ΔCu:ΔP trends across our individual experiments (Fig. 5). Offshore in Inc 1, ΔCu:ΔP was relatively constant across all Fe treatments, with no evidence for growth rate dilution or dependence upon initial Cu:P (Figs. 5, S4). In Inc 2 inshore, on the other hand, there was a large range in ΔCu:ΔP that encompassed the other incubations and was more strongly influenced by initial Cu:P differences (Fig. 5). In Inc 3, the unamended offshore waters had ΔCu:ΔP similar to the suite of Inc 1 treatments, whereas the 50:50 mix with inshore waters had higher ΔCu:ΔP that reflected an increase in ΔCu:ΔP with increased initial Cu:P from the inshore waters (Fig. 5).

The higher apparent ΔCu:ΔP relative to initial Cu:P offshore may reflect the observed differences in diatom communities between the inshore and offshore incubations. Oceanic diatoms in the offshore incubations were likely smaller, with higher surface area to volume ratios, and were growing in a very low Mn (potentially Fe–Mn colimiting) environment. Efforts to acquire sufficient Mn may have led to higher Cu:P uptake relative to the initial Cu:P. Inshore, larger diatoms growing in waters replete with bioavailable Mn, Zn, and Cd, would have lower diffusive fluxes of Cu to cell surface uptake sites that were also more frequently occupied with the target nutrient elements (i.e., Mn, Zn, Cd). The higher bioavailability of dissolved Cu in these inshore waters, however, led to higher ΔCu:ΔP as initial Cu:P increased in these treatments. In combination, our results suggest that ΔCu:ΔP was influenced both by distinctions in bioavailability of dissolved Cu in inshore relative to offshore waters and by differences in the diatom communities that dominated inshore vs. offshore experiments.

Bioavailability, substitution, and recycling

With the exception of Fe in the unamended offshore incubations, the concentrations of every trace metal we measured declined in the light over the course of our incubation experiments, consistent with strong biological demand for these elements. Tracking changes in dissolved trace metals and macronutrients during our incubations provided novel insights into the bioavailability of trace metals in offshore and inshore waters of the Southern Ocean.

We observed rapid and near-complete drawdown of dissolved Mn across both inshore and offshore experiments in light bottles (Table S11), suggesting that Mn was highly bioavailable. Dissolved Zn, Cd, and Co were also drawn down extensively with phytoplankton growth in all three incubations. In the case of Zn and Cd, dissolved concentration declines (ΔZn, ΔCd) were roughly equivalent to Zn′ and Cd′ concentrations determined from speciation measurements of the Drake Passage water column (Baars and Croot 2011; Baars et al. 2014), suggesting that organic complexation is a governing factor of their bioavailability. This may be especially important for Zn, which was depleted to a similar (1–2 nmol L^{-1}) threshold across the three experiments, after which phosphate, silicic acid, and other metals continued to decline (Figs. 2–4). Organic complexation of Zn may also be important driver of Co demand in these waters, as although we observed a similar magnitude of Co depletion as seen in a seasonal study in the Ross Sea (Saito et al. 2010) there was an apparent delay of Co uptake relative to Zn in the experiments.

Organic complexation of Cu and Ni were also likely important drivers of bioavailability. Percent drawdown of both elements was very low overall and concentration declines were not measured until later in the incubations compared to the other trace metals. Higher concentrations of both elements were drawn down from the unamended Inc 2 waters compared to offshore waters, consistent with the weaker organic complexation of Cu reported for inshore waters (Bundy et al. 2013). There are no Ni speciation data from the Southern Ocean, but Ni concentration distributions are similar to Cu, and the organic ligands governing Cu speciation may also bind Ni (Boiteau et al. 2016). Relative to changes in the dark, we saw that Fe was drawn down earliest (but only in the high Fe treatments), then drawdown of Mn and Zn occurred across all treatments, followed by Cd, and then Co, Cu, and Ni.

Free Mn, Zn, and Cd concentrations can also play a role in determining ΔM:ΔP of these elements through competition at their non-specific transport systems on cell surfaces (Sunda and Huntsman 1996, 1998, 2000). Our offshore incubations

Table 2. Phytoplankton nutrient quotas in our incubation treatments based on ΔSi:ΔP, ΔN:ΔP, and ΔM:ΔP calculated from dissolved concentration changes in incubation bottles that were sampled on both T_0 and T_{final} for each treatment. The lack of apparent Fe drawdown in the low Fe incubations led to negative cellular quotas for the essential element, suggesting Fe regenerated from biogenic pools was an important Fe sources for growth (*see* main text); these values are noted in red in the table.

	Treatment	Nutrient quotas in bottles sampled both at T_0 and T_{final}
Inc 1	+0 offshore	$(Si_{17.4}\ N_{11}\ P)_{1000}\ Zn_{2.73}\ Ni_{0.56}\ Mn_{0.47}\ Cd_{0.35}\ Cu_{0.26}\ Co_{0.01}\ Fe_{-0.16}$
	+600 pmol L^{-1} B_{12}	$(Si_{18.1}\ N_{12.2}\ P)_{1000}\ Zn_{2.38}\ Ni_{0.42}\ Mn_{0.4}\ Cd_{0.31}\ Cu_{0.25}\ Co_{0.008}\ Fe_{-0.26}$
	+1 nmol L^{-1} $^{57}FeCl_3$	$(Si_{18.4}\ N_{15.1}\ P)_{1000}\ Zn_{2.4}\ Ni_{0.54}\ Mn_{0.36}\ Fe_{0.32}\ Cd_{0.31}\ Cu_{0.28}\ Co_{0.014}$
	+4 nmol L^{-1} $^{57}FeCl_3$	$(Si_{19.7}\ N_{15.9}\ P)_{1000}\ Zn_{2.37}\ Fe_{1.66}\ Ni_{0.5}\ Mn_{0.36}\ Cd_{0.32}\ Cu_{0.25}\ Co_{0.013}$
	+600 pmol L^{-1} B_{12} + 4 nmol L^{-1} $^{57}FeCl_3$	$(Si_{20.2}\ N_{16}\ P)_{1000}\ Zn_{2.12}\ Fe_{1.06}\ Ni_{0.6}\ Mn_{0.32}\ Cd_{0.29}\ Cu_{0.26}\ Co_{0.035}$
	+10 nmol L^{-1} $^{57}FeCl_3$	$(Si_{19.1}\ N_{15.3}\ P)_{1000}\ Fe_{3.56}\ Zn_{2.19}\ Ni_{0.63}\ Mn_{0.33}\ Cd_{0.3}\ Cu_{0.24}\ Co_{0.017}$
Inc 2	+0 inshore	$(Si_{21.5}\ N_{16.3}\ P)_{1000}\ Fe_{2.19}\ Zn_{2.08}\ Mn_{1.99}\ Ni_{0.55}\ Cd_{0.31}\ Cu_{0.26}\ Co_{0.036}$
	+600 pmol L^{-1} B_{12}	$(Si_{22.3}\ N_{16.7}\ P)_{1000}\ Fe_{2.34}\ Zn_{2.25}\ Mn_{1.97}\ Ni_{0.36}\ Cd_{0.28}\ Cu_{0.18}\ Co_{0.06}$
	+4 nmol L^{-1} $^{57}FeCl_3$	$(Si_{20.5}\ N_{16.6}\ P)_{1000}\ Fe_{2.95}\ Zn_{2.7}\ Mn_{2.03}\ Ni_{0.52}\ Cd_{0.31}\ Cu_{0.2}\ Co_{0.032}$
Inc 3	+0 offshore	$(Si_{14.3}\ N_{13.2}\ P)_{1000}\ Zn_{3.03}\ Ni_{0.57}\ Mn_{0.49}\ Cd_{0.38}\ Cu_{0.25}\ Co_{0.021}\ Fe_{-0.18}$
	50:50 mix offshore : filtered inshore	$(N_{15.8}\ Si_{15.1}\ P)_{1000}\ Zn_{2.15}\ Mn_{1.16}\ Fe_{0.75}\ Cu_{0.35}\ Ni_{0.29}\ Cd_{0.28}\ Co_{0.023}$

were Fe-limited with low Mn and high Zn and Cd (Fig. 4). We observed preferential uptake of all three of these metals relative to P in the Fe-limited treatments, and growth rate dilution of metal uptake between Fe-limited and Fe-replete treatments. Inshore, all three trace elements were present at elevated concentrations, with higher Zn and especially Mn inshore (Fig. 4). Of the three elements, Mn was the only metal drawn down preferentially over P in the intermediate timepoints inshore (Fig. S3), which allowed ΔMn:ΔP to ultimately remain tightly correlated with initial Mn:P concentrations independent of growth rates (Fig. 5; Table 1).

In contrast, for Cd and Zn, differences in the bioavailability of Cd and Zn, and perhaps in the differential regeneration of these elements (Collier and Edmond 1984; Hollister et al. 2020), may have had a greater influence on their respective uptake, and especially Co uptake, in these experiments. In the Fe-replete and Fe-amended treatments of all three incubations, the largest declines in Co were observed between the last two timepoints of the experiments as Zn concentrations plateaued (Figs. 3, 4) and Cd was first preferentially taken up over Zn (Fig. S7). We also observed that the total Co uptake (ΔCo:ΔP) was higher in treatments with high growth rates and the lowest ΔCd:ΔP and ΔZn:ΔP uptake (Fig. S4; Table 1), consistent with Co substitution for Zn (Morel et al. 2020).

Organic complexation of Fe in the marine environment is widespread, and an important environmental adaptation to the exceedingly low solubility of Fe′ in seawater. We have not measured Fe-binding organic ligands in our incubation samples, but we expect that Fe speciation in these waters is similar to other regions of the Southern Ocean and governed by strong organic ligands (Buck et al. 2010). Organic complexation reduces Fe bioavailability relative to Fe′ but since nearly all dissolved Fe in seawater is organically complexed (Gledhill and Buck 2012), phytoplankton have adapted to access this pool and organically complexed Fe is typically bioavailable to phytoplankton (Shaked et al. 2020). Nevertheless, we observed no apparent drawdown of dissolved Fe in our unamended offshore incubation experiments (Fig. 3). Dissolved Fe additions, whether as inorganic $^{57}FeCl_3$ (Inc 1) or as a mix with naturally Fe-rich water (Inc 3) were rapidly drawn down by the offshore communities and led to much higher ΔFe:ΔP compared to low Fe controls (Table 1). Contamination was not obvious in any of the experiments, and we posit that the phytoplankton growth in the Fe-limited incubations offshore was supported by recycling of Fe from biogenic particulate phases, which was more bioavailable than the dissolved Fe pool we measured in the incubation bottles. This is a surprising finding, as we observed significant biomass accumulation and nitrate drawdown without a new Fe source in these treatments (Fig. 2), but it is also consistent with insights from previous studies in the Southern Ocean (de Jong et al. 2012; Sieber et al. 2020) and Fe-limited Equatorial Pacific (Rafter et al. 2017).

We suspect that recycling of other trace metals from biogenic phases was also important in our experiments. Our estimates of cellular elemental quotas (Table 2) from dissolved inventory changes were typically much lower than direct measurements of quotas in Southern Ocean diatom cells (Twining and Baines 2013). This discrepancy between dissolved metal uptake and particulate cellular content exists across multiple studies in the Southern Ocean, with estimates of cellular metal quotas based on dissolved uptake consistent with each other but typically much lower than particulate measurements (*see* Table 1 and references therein). Reconciling this difference is important for advancing our understanding of Southern Ocean trace metal cycling.

Relationship to the Southern Ocean system

The Southern Ocean serves as a hub of the global overturning circulation (Talley 2013), with nutrient-rich deep water upwelled to the surface of the ACC in a spiraling

pathway of topographically defined "hotspots" that include Drake Passage (Tamsitt et al. 2017). In addition to supplying macronutrients, results from our experiments suggest that this upwelling is an important source of bioavailable forms of trace metals to support the growth of local phytoplankton communities in austral spring.

Biogeochemical processes occurring in the Southern Ocean also have an outsized influence on the global ocean via the formation of intermediate and bottom waters here and their subsequent advection to lower latitudes (Broecker et al. 1998; Sarmiento et al. 2004; Marinov et al. 2006). The Drake Passage water of this study feeds partly into the Weddell Sea, where Antarctic Bottom Water is formed, sinks, and is then transported north (Talley 2013). We document the rapid depletion of bioavailable pools of dissolved trace metals during spring phytoplankton growth in the ACC and over the WAP shelf. In particular, we suggest that secondary Mn limitation and depletion of bioavailable Zn in the Southern Ocean drives the ordering of the depletion of other trace metals as phytoplankton growth progresses, and that the absence of Mn oxidation may facilitate efficient recycling of trace metals from biogenic particles that may have otherwise been lost to scavenging. Our observations of efficient recycling of at least biogenic Fe to support spring growth and the apparent substitution of Co for Zn despite residual pools of dissolved Fe, Zn, and Cd in all three experiments suggest that inventories of these trace metals remaining in surface waters following spring diatom growth are entrained into subsurface water masses formed in this region as preformed micronutrients that may have limited bioavailability to phytoplankton communities downstream.

We also acknowledge that grazers, mixed layer depth changes, and position of Southern Ocean fronts (i.e., latitude) may all affect nutrient and trace metal cycling (Viljoen et al. 2019), and influence air–sea carbon exchange and preformed nutrient delivery to lower latitudes (Marinov et al. 2006). Our incubation experiments did not capture these factors but did allow us to identify aspects of trace metal feedbacks with natural phytoplankton assemblages that inform our understanding of biogeochemical processes happening in the Southern Ocean. As preformed nutrient concentrations indirectly govern atmospheric carbon dioxide concentrations (Marinov et al. 2006), and trace metals are important drivers of community structure and ocean productivity (Sunda 1989; Morel and Price 2003), preformed trace metal concentrations and their relative bioavailability are crucial considerations for the global carbon cycle and climate.

Data availability statement

Chlorophyll, macronutrient, and trace metal data from the three incubation experiments are available through the NSF Biological & Chemical Oceanography Data Management Office (BCO-DMO) (Buck et al. 2018*a*, 2019*a*,*b*,*c*; Chappell et al. 2022).

References

Archer, C., D. Vance, A. Milne, and M. C. Lohan. 2020. The oceanic biogeochemistry of nickel and its isotopes: New data from the South Atlantic and the Southern Ocean biogeochemical divide. Earth Planet. Sci. Lett. **535**: 116118. doi:10.1016/j.epsl.2020.116118

Baars, O., and P. L. Croot. 2011. The speciation of dissolved zinc in the Atlantic sector of the Southern Ocean. Deep-Sea Res. II Top. Stud. Oceanogr. **58**: 2720–2732. doi:10.1016/j.dsr2.2011.02.003

Baars, O., W. Abouchami, S. J. G. Galer, M. Boye, and P. L. Croot. 2014. Dissolved cadmium in the Southern Ocean: Distribution, speciation, and relation to phosphate. Limnol. Oceanogr. **59**: 385–399. doi:10.4319/lo.2014.59.2.0385

Bertrand, E. M., M. A. Saito, J. M. Rose, C. R. Riesselman, M. C. Lohan, A. E. Noble, P. A. Lee, and G. R. DiTullio. 2007. Vitamin B_{12} and iron colimitation of phytoplankton growth in the Ross Sea. Limnol. Oceanogr. **52**: 1079–1093. doi:10.4319/lo.2007.52.3.1079

Bertrand, E. M., M. A. Saito, P. A. Lee, R. B. Dunbar, P. N. Sedwick, and G. R. Ditullio. 2011. Iron limitation of a springtime bacterial and phytoplankton community in the Ross Sea: Implications for vitamin B_{12} nutrition. Front. Microbiol. **2**: 160. doi:10.3389/fmicb.2011.00160

Biller, D. V., and K. W. Bruland. 2012. Analysis of Mn, Fe, Co, Ni, Cu, Zn, Cd, and Pb in seawater using the Nobias-chelate PA1 resin and magnetic sector inductively coupled plasma mass spectrometry (ICP-MS). Mar. Chem. **130**: 12–20. doi:10.1016/j.marchem.2011.12.001

Boiteau, R. M., and others. 2016. Structural characterization of natural nickel and copper binding ligands along the US GEOTRACES eastern Pacific zonal transect. Front. Mar. Sci. **3**: 243. doi:10.3389/fmars.2016.00243

Bown, J., P. Laan, S. Ossebaar, K. Bakker, P. Rozema, and H. J. W. de Baar. 2017. Bioactive trace metal time series during austral summer in Ryder Bay, Western Antarctic Peninsula. Deep-Sea Res. II Top. Stud. Oceanogr. **139**: 103–119. doi:10.1016/j.dsr2.2016.07.004

Boyd, P. W., and others. 2000. A mesoscale phytoplankton bloom in the polar Southern Ocean stimulated by iron fertilization. Nature **407**: 695–702. doi:10.1038/35037500

Boyd, P. W., and others. 2007. Mesoscale iron enrichment experiments 1993–2005: Synthesis and future directions. Science **315**: 612–617. doi:10.1126/science.1131669

Brand, L. E., W. G. Sunda, and R. R. L. Guillard. 1983. Limitation of marine phytoplankton reproductive rates by zinc, manganese, and iron. Limnol. Oceanogr. **28**: 1182–1198. doi:10.4319/lo.1983.28.6.1182

Broecker, W. S., and others. 1998. How much deep water is formed in the Southern Ocean? J. Geophys. Res.: Oceans **103**: 15833–15843. doi:10.1029/98jc00248

Browning, T. J., E. P. Achterberg, A. Engel, and E. Mawji. 2021. Manganese co-limitation of phytoplankton growth

and major nutrient drawdown in the Southern Ocean. Nat. Commun. **12**: 884. doi:10.1038/s41467-021-21122-6

Bruland, K. W. 1980. Oceanographic distributions of cadmium, zinc, nickel, and copper in the North Pacific. Earth Planet. Sci. Lett. **47**: 176–198. doi:10.1016/0012-821X(80)90035-7

Bruland, K. W., J. R. Donat, and D. A. Hutchins. 1991. Interactive influences of bioactive trace metals on biological production in oceanic waters. Limnol. Oceanogr. **36**: 1555–1577. doi:10.4319/lo.1991.36.8.1555

Buck, K. N., K. E. Selph, and K. A. Barbeau. 2010. Iron-binding ligand production and copper speciation in an incubation experiment of Antarctic Peninsula shelf waters from the Bransfield Strait, Southern Ocean. Mar. Chem. **122**: 148–159. doi:10.1016/j.marchem.2010.06.002

Buck, K., P. Chappell, and B. Jenkins. 2018*a*. Dissolved macronutrient concentrations from incubation experiments performed on RVIB Nathaniel B. Palmer cruise NBP 16-08 from September to October 2016. Biological and Chemical Oceanography Data Management Office (BCO-DMO). 10.1575/1912/bco-dmo.743072.1

Buck, K. N., P. N. Sedwick, B. Sohst, and C. A. Carlson. 2018*b*. Organic complexation of iron in the eastern tropical South Pacific: Results from US GEOTRACES Eastern Pacific Zonal Transect (GEOTRACES cruise GP16). Mar. Chem. **201**: 229–241. doi:10.1016/j.marchem.2017.11.007

Buck, K., P. Chappell, and B. Jenkins. 2019*a*. Dissolved trace metal concentrations for Incubation 1, initiated September 11th, 2016 on RVIB Nathaniel B. Palmer cruise NBP16-08 in the Southern Ocean. Biological and Chemical Oceanography Data Management Office (BCO-DMO). 10.1575/1912/bco-dmo.781759.1

Buck, K., P. Chappell, and B. Jenkins. 2019*b*. Dissolved trace metal concentrations for Incubation 2, initiated September 24th, 2016 on RVIB Nathaniel B. Palmer cruise NBP16-08 in the Southern Ocean. Biological and Chemical Oceanography Data Management Office (BCO-DMO). 10.1575/1912/bco-dmo.781827.1

Buck, K., P. Chappell, and B. Jenkins. 2019*c*. Dissolved trace metal concentrations for Incubation 3, initiated September 27th, 2016 on RVIB Nathaniel B. Palmer cruise NBP16-08 in the Southern Ocean. Biological and Chemical Oceanography Data Management Office (BCO-DMO). 10.1575/1912/bco-dmo.781841.1

Bundy, R. M., K. A. Barbeau, and K. N. Buck. 2013. Sources of strong copper-binding ligands in Antarctic Peninsula surface waters. Deep-Sea Res. II Top. Stud. Oceanogr. **90**: 134–146. doi:10.1016/j.dsr2.2012.07.023

Capodaglio, G., C. Turetta, G. Toscano, A. Gambaro, G. Scarponi, and P. Cescon. 1998. Cadmium, lead and copper complexation in Antarctic coastal seawater. Evolution during the austral summer. Int. J. Environ. Anal. Chem. **71**: 195–226. doi:10.1080/03067319808032628

Chappell, P. D., K. Buck, and B. D. Jenkins. 2022. Chlorophyll and phaeopigment concentrations from incubation experiments performed with amended Southern Drake Passage on RVIB Nathaniel B. Palmer cruise NBP 16-08 from September to October 2016. Biological and Chemical Oceanography Data Management Office (BCO-DMO). 10.26008/1912/bco-dmo.742206.1

Cheize, M., and others. 2019. Contribution of resuspended sedimentary particles to dissolved iron and manganese in the ocean: An experimental study. Chem. Geol. **511**: 389–415. doi:10.1016/j.chemgeo.2018.10.003

Collier, R., and J. Edmond. 1984. The trace element geochemistry of marine biogenic particulate matter. Prog. Oceanogr. **13**: 113–199. doi:10.1016/0079-6611(84)90008-9

Croft, M. T., A. D. Lawrence, E. Raux-Deery, M. J. Warren, and A. G. Smith. 2005. Algae acquire vitamin B_{12} through a symbiotic relationship with bacteria. Nature **438**: 90–93. doi:10.1038/nature04056

Croot, P. L., O. Baars, and P. Streu. 2011. The distribution of dissolved zinc in the Atlantic sector of the Southern Ocean. Deep-Sea Res. II Top. Stud. Oceanogr. **58**: 2707–2719. doi:10.1016/j.dsr2.2010.10.041

Cullen, J. T., Z. Chase, K. H. Coale, S. E. Fitzwater, and R. M. Sherrell. 2003. Effect of iron limitation on the cadmium to phosphorus ratio of natural phytoplankton assemblages from the Southern Ocean. Limnol. Oceanogr. **48**: 1079–1087. doi:10.4319/lo.2003.48.3.1079

Cutter, G. A., and K. W. Bruland. 2012. Rapid and noncontaminating sampling system for trace elements in global ocean surveys. Limnol. Oceanogr.: Methods **10**: 425–436. doi:10.4319/lom.2012.10.425

de Baar, H. J. W.., and others. 2005. Synthesis of iron fertilization experiments: From the iron age in the age of enlightenment. J. Geophys. Res.: Oceans **110**: C09S16. doi:10.1029/2004jc002601

de Baar, H. J. W., A. G. J. Buma, R. F. Nolting, G. C. Cadee, G. Jacques, and P. J. Treguer. 1990. On iron limitation of the Southern Ocean: Experimental observations in the Weddell and Scotia Seas. Mar. Ecol. Prog. Ser. **65**: 105–122. doi:10.3354/meps065105

de Jong, J., V. Schoemann, D. Lannuzel, P. Croot, H. de Baar, and J.-L. Tison. 2012. Natural iron fertilization of the Atlantic sector of the Southern Ocean by continental shelf sources of the Antarctic Peninsula. J. Geophys. Res.: Biogeosci. **117**: G01029. doi:10.1029/2011jg001679

Fischer, A. C., J. J. Kroon, T. G. Verburg, T. Teunissen, and H. T. Wolterbeek. 2007. On the relevance of iron adsorption to container materials in small-volume experiments on iron marine chemistry: ^{55}Fe-aided assessment of capacity, affinity and kinetics. Mar. Chem. **107**: 533–546. doi:10.1016/j.marchem.2007.08.004

Fitzsimmons, J. N., and E. A. Boyle. 2012. An intercalibration between the GEOTRACES GO-FLO and the MITESS/vanes sampling systems for dissolved iron concentration analyses

(and a closer look at adsorption effects). Limnol. Oceanogr.: Methods **10**: 437–450. doi:10.4319/lom.2012.10.437

Gledhill, M., and K. N. Buck. 2012. The organic complexation of iron in the marine environment: A review. Front. Microbiol. **3**: 69. doi:10.3389/fmicb.2012.00069

Gordon, L. I., J. C. Jennings, A. A. Ross, and J. M. Krest. 1993. A suggested protocol for continuous flow automated analysis of seawater nutrients (phosphate, nitrate, nitrite and silicic acid) in the WOCE Hydrographic Program and the Joint Global Ocean Fluxes Study.

Hatta, M., C. I. Measures, K. E. Selph, M. Zhou, and W. T. Hiscock. 2013. Iron fluxes from the shelf regions near the South Shetland Islands in the Drake Passage during the austral-winter 2006. Deep-Sea Res. II Top. Stud. Oceanogr. **90**: 89–101. doi:10.1016/j.dsr2.2012.11.003

Helbling, E. W., V. Villafañe, and O. Holm-Hansen. 1991. Effect of iron on productivity and size distribution of Antarctic phytoplankton. Limnol. Oceanogr. **36**: 1879–1885. doi:10.4319/lo.1991.36.8.1879

Hollister, A. P., and others. 2020. Regeneration of macronutrients and trace metals during phytoplankton decay: An experimental study. Limnol. Oceanogr. **65**: 1936–1960. doi:10.1002/lno.11429

Hopkinson, B. M., and others. 2007. Iron limitation across chlorophyll gradients in the southern Drake Passage: Phytoplankton responses to iron addition and photosynthetic indicators of iron stress. Limnol. Oceanogr. **52**: 2540–2554. doi:10.4319/lo.2007.52.6.2540

Janssen, D. J., and others. 2020. Trace metal and nutrient dynamics across broad biogeochemical gradients in the Indian and Pacific sectors of the Southern Ocean. Mar. Chem. **221**: 103773. doi:10.1016/j.marchem.2020.103773

Jensen, L. T., N. J. Wyatt, W. M. Landing, and J. N. Fitzsimmons. 2020. Assessment of the stability, sorption, and exchangeability of marine dissolved and colloidal metals. Mar. Chem. **220**: 103754. doi:10.1016/j.marchem.2020.103754

Jesperson, A.-M., and K. Christoffersen. 1987. Measurements of chlorophyll-a from phytoplankton using ethanol as extraction solvent. Arch. Hydrobiol. **109**: 445–454. doi:10.1127/archiv-hydrobiol/109/1987/445

Johnson, K. S., and others. 2007. Developing standards for dissolved iron in seawater. EOS **88**: 131–132. doi:10.1029/2007EO110003

Lagerström, M., M. Field, M. Séguret, L. Fischer, S. Hann, and R. Sherrell. 2013. Automated on-line flow-injection ICP-MS determination of trace metals (Mn, Fe, Co, Ni, Cu and Zn) in open ocean seawater: Application to the GEOTRACES program. Mar. Chem. **155**: 71–80. doi:10.1016/j.marchem.2013.06.001

Löscher, B. M. 1999. Relationships among Ni, Cu, Zn, and major nutrients in the Southern Ocean. Mar. Chem. **67**: 67–102. doi:10.1016/s0304-4203(99)00050-x

Marinov, I., A. Gnanadesikan, J. R. Toggweiler, and J. L. Sarmiento. 2006. The Southern Ocean biogeochemical divide. Nature **441**: 964–967. doi:10.1038/nature04883

Martin, J. H., S. E. Fitzwater, and M. Gordon. 1990*a*. Iron deficiency limits phytoplankton growth in Antarctic waters. Glob. Biogeochem. Cycles **4**: 5–12. doi:10.1029/GB004i001p00005

Martin, J. M., R. M. Gordon, and S. E. Fitzwater. 1990*b*. Iron in Antarctic waters. Nature **345**: 156–158. doi:10.1038/345156a0

Mellett, T., and others. 2018. The biogeochemical cycling of iron, copper, nickel, cadmium, manganese, cobalt, lead, and scandium in a California Current experimental study. Limnol. Oceanogr. **63**: S425–S447. doi:10.1002/lno.10751

Middag, R., H. J. W. de Baar, P. Laan, P. H. Cai, and J. C. van Ooijen. 2011. Dissolved manganese in the Atlantic sector of the Southern Ocean. Deep-Sea Res. II Top. Stud. Oceanogr. **58**: 2661–2677. doi:10.1016/j.dsr2.2010.10.043

Middag, R., H. J. W. de Baar, M. B. Klunder, and P. Laan. 2013. Fluxes of dissolved aluminum and manganese to the Weddell Sea and indications for manganese co-limitation. Limnol. Oceanogr. **58**: 287–300. doi:10.4319/lo.2013.58.1.0287

Moore, J. K., S. C. Doney, D. M. Glover, and I. Y. Fung. 2001. Iron cycling and nutrient-limitation patterns in surface waters of the World Ocean. Deep-Sea Res. II Top. Stud. Oceanogr. **49**: 463–507. doi:10.1016/S0967-0645(01)00109-6

Moore, C. M., and others. 2013. Processes and patterns of oceanic nutrient limitation. Nat. Geosci. **6**: 701–710. doi:10.1038/ngeo1765

Morel, F., and N. Price. 2003. The biogeochemical cycles of trace metals in the oceans. Science **300**: 944–947. doi:10.1126/science.1083545

Morel, F. M. M., P. J. Lam, and M. A. Saito. 2020. Trace metal substitution in marine phytoplankton. Annu. Rev. Earth Planet. Sci. **48**: 491–517. doi:10.1146/annurev-earth-053018-060108

Morison, F., and S. Menden-Deuer. 2015. Early spring phytoplankton dynamics in the subpolar North Atlantic: The influence of protistan herbivory. Limnol. Oceanogr. **60**: 1298–1313. doi:10.1002/lno.10099

Nolting, R. F., and H. J. W. De Baar. 1994. Behaviour of nickel, copper, zinc and cadmium in the upper 300 m of a transect in the Southern Ocean (57°–62°S, 49°W). Mar. Chem. **45**: 225–242. doi:10.1016/0304-4203(94)90006-x

Oldham, V. E., R. Chmiel, C. M. Hansel, G. R. DiTullio, D. Rao, and M. Saito. 2021. Inhibited manganese oxide formation hinders cobalt scavenging in the Ross Sea. Glob. Biogeochem. Cycles **35**: e2020GB006706. doi:10.1029/2020gb006706

Panzeca, C., A. Tovar-Sanchez, S. Agustí, I. Reche, C. M. Duarte, G. T. Taylor, and S. A. Sañudo-Wilhelmy. 2006. B vitamins as regulators of phytoplankton dynamics. EOS **87**: 596. doi:10.1029/2006EO520001

Parsons, T. R., Y. Maita, and C. M. Lalli. 1984. A manual of chemical and biological methods for seawater analysis. Pergamon.

Pausch, F., K. Bischof, and S. Trimborn. 2019. Iron and manganese co-limit growth of the Southern Ocean diatom *Chaetoceros debilis*. PLoS One **14**: e0221959. doi:10.1371/journal.pone.0221959

Price, N. M., and F. M. M. Morel. 1990. Cadmium and cobalt substitution for zinc in a marine diatom. Nature **344**: 658–660. doi:10.1038/344658a0

Rafter, P. A., D. M. Sigman, and K. R. M. Mackey. 2017. Recycled iron fuels new production in the eastern equatorial Pacific Ocean. Nat. Commun. **8**: 1100. doi:10.1038/s41467-017-01219-7

Saito, M. A., T. J. Goepfert, and J. T. Ritt. 2008. Some thoughts on the concept of colimitation: Three definitions and the importance of bioavailability. Limnol. Oceanogr. **53**: 276–290. doi:10.4319/lo.2008.53.1.0276

Saito, M. A., T. J. Goepfert, A. E. Noble, E. M. Bertrand, P. N. Sedwick, and G. R. Ditullio. 2010. A seasonal study of dissolved cobalt in the Ross Sea, Antarctica: Micronutrient behavior, absence of scavenging, and relationships with Zn, Cd, and P. Biogeosciences **7**: 4059–4082. doi:10.5194/bg-7-4059-2010

Sañudo-Wilhelmy, S. A., C. J. Gobler, M. Okbamichael, and G. T. Taylor. 2006. Regulation of phytoplankton dynamics by vitamin B_{12}. Geophys. Res. Lett. **33**: L04604. doi:10.1029/2005gl025046

Sarmiento, J., N. Gruber, M. Brzezinski, and J. Dunne. 2004. High-latitude controls of thermocline nutrients and low latitude biological productivity. Nature **427**: 56–60. doi:10.1038/nature02127

Shaked, Y., K. N. Buck, T. Mellett, and M. T. Maldonado. 2020. Insights into the bioavailability of oceanic dissolved Fe from phytoplankton uptake kinetics. ISME J. **14**: 1182–1193. doi:10.1038/s41396-020-0597-3

Sherrell, R. M., M. E. Lagerström, K. O. Forsch, S. E. Stammerjohn, and P. L. Yager. 2015. Dynamics of dissolved iron and other bioactive trace metals (Mn, Ni, Cu, Zn) in the Amundsen Sea Polynya, Antarctica. Elementa **3**: 000071. doi:10.12952/journal.elementa.000071

Sieber, M., T. M. Conway, G. F. de Souza, C. S. Hassler, M. J. Ellwood, and D. Vance. 2020. Cycling of zinc and its isotopes across multiple zones of the Southern Ocean: Insights from the Antarctic circumnavigation expedition. Geochim. Cosmochim. Acta **268**: 310–324. doi:10.1016/j.gca.2019.09.039

Sieber, M., T. M. Conway, G. F. de Souza, C. S. Hassler, M. J. Ellwood, and D. Vance. 2021. Isotopic fingerprinting of biogeochemical processes and iron sources in the iron-limited surface Southern Ocean. Earth Planet. Sci. Lett. **567**: 116967. doi:10.1016/j.epsl.2021.116967

Sohrin, Y., S. Urushihara, S. Nakatsuka, T. Kono, E. Higo, T. Minami, K. Norisuye, and S. Umetani. 2008. Multielemental determination of GEOTRACES key trace metals in seawater by ICPMS after preconcentration using an ethylenediaminetriacetic acid chelating resin. Anal. Chem. **80**: 6267–6273. doi:10.1021/ac800500f

Sterling, A. R., L. Z. Holland, R. M. Bundy, S. M. Burns, K. N. Buck, P. D. Chappell, and B. D. Jenkins. 2022. Potential interactions between diatoms and bacteria are shaped by trace element gradients in the Southern Ocean. Front. Mar. Sci. doi:10.3389/fmars.2022.876830

Sunda, W. G. 1989. Trace metal interactions with marine phytoplankton. Biol. Oceanogr. **6**: 411–442. doi:10.1080/01965581.1988.10749543

Sunda, W. G., and S. A. Huntsman. 1995. Iron uptake and growth limitation in oceanic and coastal phytoplankton. Mar. Chem. **50**: 189–206. doi:10.1016/0304-4203(95)00035-P

Sunda, W. G., and S. A. Huntsman. 1996. Antagonisms between cadmium and zinc toxicity and manganese limitation in a coastal diatom. Limnol. Oceanogr. **41**: 373–387. doi:10.4319/lo.1996.41.3.0373

Sunda, W. G., and S. A. Huntsman. 1998. Control of Cd concentrations in a coastal diatom by interactions among free ionic Cd, Zn, and Mn in seawater. Environ. Sci. Technol. **32**: 2961–2968. doi:10.1021/es980271y

Sunda, W. G., and S. A. Huntsman. 2000. Effect of Zn, Mn, and Fe on Cd accumulation in phytoplankton: Implications for oceanic Cd cycling. Limnol. Oceanogr. **45**: 1501–1516. doi:10.4319/lo.2000.45.7.1501

Talley, L. 2013. Closure of the global overturning circulation through the Indian, Pacific, and southern oceans: Schematics and transports. Oceanography **26**: 80–97. doi:10.5670/oceanog.2013.07

Tamsitt, V., and others. 2017. Spiraling pathways of global deep waters to the surface of the Southern Ocean. Nat. Commun. **8**: 172. doi:10.1038/s41467-017-00197-0

Twining, B. S., and S. B. Baines. 2013. The trace metal composition of marine phytoplankton. Ann. Rev. Mar. Sci. **5**: 191–215. doi:10.1146/annurev-marine-121211-172322

Twining, B. S., S. B. Baines, S. Vogt, and D. M. Nelson. 2012. Role of diatoms in nickel biogeochemistry in the ocean. Glob. Biogeochem. Cycles **26**: GB4001. doi:10.1029/2011gb004233

Viljoen, J. J., I. Weir, S. Fietz, R. Cloete, J. Loock, R. Philibert, and A. N. Roychoudhury. 2019. Links between the phytoplankton community composition and trace metal distribution in summer surface waters of the Atlantic Southern Ocean. Front. Mar. Sci. **6**: 295. doi:10.3389/fmars.2019.00295

Wood, A. M., R. C. Everroad, and L. M. Wingard. 2005. Measuring growth rates in microalgal cultures, p. 269–288. *In* R. A. Andersen [ed.], Algal culturing techniques. Academic Press.

Wu, M., J. S. P. McCain, E. Rowland, R. Middag, M. Sandgren, A. E. Allen, and E. M. Bertrand. 2019. Manganese and iron deficiency in Southern Ocean *Phaeocystis antarctica* populations revealed through taxon-specific protein indicators. Nat. Commun. **10**: 3582. doi:10.1038/s41467-019-11426-z

Acknowledgments

This work was supported by funding from the U.S. National Science Foundation: NSF OPP-1443483 to KNB, NSF OPP-1443474 to BDJ, and NSF OPP-1443646 to PDC. We declare no conflicts of interest. We thank Rob Sherrell for use of his x-Niskin samplers and the Palmer LTER program for the use of their trace metal sampling rosette. We thank Travis Mellett for mobilization assistance. We also thank the captain and crew of the R/V/I/B *Nathaniel B. Palmer*, and students Sveinn Einarsson, Noahie Encarnacion, Kristofer Gomes, Laura Holland, and PolarTrek teacher Cara Pekarcik, for help with carrying out the incubations. We thank Ana Aguilar-Islas, Jessica Fitzsimmons, Laramie Jensen, and Angie Milne for their assistance with seaFAST method development and Salvatore Caprara, Ethan Goddard, and Kelly Deister for Element XR ICP-MS assistance at USF.

Conflict of Interest

None declared.

Submitted 14 January 2022
Revised 05 October 2022
Accepted 07 December 2022

Associate editor: Vanessa Hatje